2006

Experimental Study of the Entrainment of Nanoparticles from Surfaces

Srirupa Ganguly
Virginia Commonwealth University

School of Engineering
Virginia Commonwealth University

This is to certify that the thesis prepared by Srirupa Ganguly entitled EXPERIMENTAL STUDY OF THE ENTRAINMENT OF NANOPARTICLES FROM SURFACES has been approved by her committee as satisfactory completion of the thesis or dissertation requirement for the degree of Master of Science in Engineering

Dr. James T. McLeskey Jr., Ph.D., Assistant Professor, Mechanical Engineering

Dr. Purusottam Jena, Ph.D., Distinguished Professor, Department of Physics

Dr. Karla M. Mossi, Ph.D., Assistant Professor, Mechanical Engineering

L. Thomas Overby, Ph.D., Assistant Dean of Graduate Affairs, School of Engineering

Russell D. Jamison, Ph.D., Dean, School of Engineering

F. Douglas Boudinot, Ph.D., Dean, School of Graduate Studies

September 29, 2006
Date

EXPERIMENTAL STUDY OF THE ENTRAINMENT OF NANOPARTICLES FROM SURFACES

A Thesis submitted in partial fulfillment of the requirements for the degree of MS at Virginia Commonwealth University.

by

SRIRUPA GANGULY
Bachelor of Engineering, R.V.C.E., Bangalore, India, 2002

Director: DR. JAMES T. MCLESKEY JR.

ASSISTANT PROFESSOR, DEPARTMENT OF MECHANICAL ENGINEERING

Virginia Commonwealth University
Richmond, Virginia
September 2006

Acknowledgment

I would like to acknowledge and thank my thesis director, Dr. James T. McLeskey Jr. for the patience, time and knowledge that he generously shared with me throughout my research. In addition to Dr. McLeskey, I would like to thank my committee members, Dr. Purusottam Jena and Dr. Karla M. Mossi who encouraged and co-operated in the development and completion of this work. I would like to thank Dr. Mohammad Hajaligol for sharing his knowledge and understanding with me, and providing me with insights that contributed immensely to the quality of this research.

I am grateful to my parents, Sipra and Shambhu Nath Ganguly, for their encouragement, love and support. Their ethical way of life and achievements in professional as well as personal life, has set a role model for me.

I would like to express my appreciation to my husband, Sanjiv Sinha, for providing encouragement, support, understanding and knowledge during this demanding project.

I would like to thank my friends and colleagues in school and PMUSA who helped me in the development of this work.

Table of Contents

Page

List of Tables

Page

List of Figures

Page

Abstract

EXPERIMENTAL STUDY OF THE ENTRAINMENT OF NANOPARTICLES FROM SURFACES

By Srirupa Ganguly, M.S.

A Thesis submitted in partial fulfillment of the requirements for the degree of M.S. at Virginia Commonwealth University.

Virginia Commonwealth University, 2006

Major Director: Dr. James T. McLeskey Jr.
Assistant Professor, Department of Mechanical Engineering

The adhesion and resuspension of nanoparticles is important in applications ranging from semiconductor manufacturing to pollution management. The objective of this work is to understand the effect of particle size on re-entrainment of nanometer scale particles. One of the major contributions is to reduce the randomness introduced in past measurements on resuspension by controlling humidity, temperature, material and the distribution of shape and particle sizes. In the process of studying particle size, the effect of surface roughness was also found. Measurements of the detachment fraction of carbon

particles as a function of flow rate show three distinct regimes that we attribute to the dominance of drag, energy accumulation by particles, and collision and agglomeration respectively. Experiments with silica nanoparticles on silica microspheres show the detachment fraction to increase non-linearly with particle diameter and to decrease with the substrate diameter. We attribute the former to the dominance of the drag moment over the adhesive moment. We attribute the influence of the substrates to the surface roughness being comparable to the size of the nanoparticles. This work provides new empirical insight into the interaction of nanoparticles with surfaces and fluid flows.

CHAPTER 1 Introduction

This work is an attempt to understand the properties and surface characteristics of nanoparticles that are in contact with surfaces. The nanoparticles are subjected to an aerodynamic removal force and their consequent detachment from the surface is studied.

1.1 Why Study Nanoparticle Entrainment from Surfaces?

Particles are present all around us, ranging from pollen, dust and fibers to metals and metal oxides. These particles are held to the surface by strong attractive forces. A control over the attachment and detachment process is important in many fields including semiconductor industry, aerosol research, pneumatic transport, design of filters, control of micro-contamination, groundwater, handling of toxic substances and oil transport (Nicholson 1988; Theerachaisupakij, Matsusaka et al. 2003). For example, in the semiconductor industry, contamination due to particle adhesion accounts for 50% of the yield loss (Hoenig 1986).

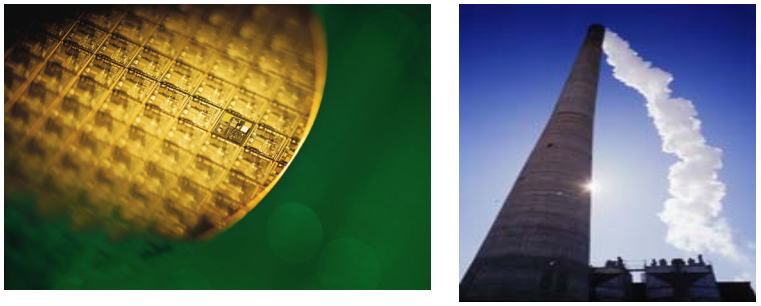

Fig. 1.1 Particle entrainment is of practical importance in semiconductors and pollution control.

The adhesion of nanoparticles to surfaces is very difficult to control. Removal of nanoparticles can be brought about by aerodynamic or hydrodynamic forces. However, the removal process becomes increasingly difficult with decreasing particle size. The removal of particles in the nanometer range puts forward a new challenge.

1.2 Statement of the Problem

The removal of nanoparticles from surfaces subjected to turbulent flow has been the focus of several theoretical and experimental studies. The variability of the properties of the particles and the ambiguous nature of the results are due to the broad distribution of particle-surface interactions. The problem can be solved by designing a study that considers particles with uniform properties in contact with a well-characterized surface.

Our goal is to perform entrainment experiments with uniform-sized spherical nanoparticles in contact with a well-characterized surface. Aerodynamic force, with well-defined flow parameters is used to detach the particles. The use of different sizes of spheres while other parameters are carefully controlled, results in a narrow distribution of sphere-surface forces (Phares, Smedley et al. 2000). This facilitates a better understanding of the process. The scientific objective is to determine the effect of particle size and surface roughness on the entrainment process. The biggest hurdle in this study is the random nature of the process and the complexity introduced by several factors such as humidity, residence time, material properties of particle and surface, and flow rate of removal force.

1.3 Organization of the Thesis

We review the theory behind the resuspension of nanoparticles from surfaces in Chapter 2. In particular, we discuss the two most commonly used models: the energy balance model and the force balance model. Chapter 3 describes the development of an experimental setup to ultimately measure the fraction of particles that are detached from a substrate due to air-flow over the substrate. We also describe the characterization of the particles and the substrates used in this work. Chapter 4 discusses experiments on the resuspension of carbon particles. This study helps to identify the key factors that introduce randomness in measurements. The insight gained from this study is used to redesign the experiments using silica particles. This is discussed in Chapter 5. We analyze the experimental data to understand the effect of particle size and surface roughness on the process of adhesion and resuspension of particles from the substrate. We present our conclusions and provide suggestions for future work in Chapter 6.

1.4 Summary

Experiments to date have involved a broad distribution of particle-surface interactions. Neither results from previous experiments nor models developed to predict the entrainment behavior have been able to satisfactorily explain the detachment of nanoparticles from surfaces subjected to airflow. Our work is an attempt to understand the entrainment process with respect to size of the nanoparticle.

CHAPTER 2 Mechanics of Resuspension

This chapter presents a survey of the literature on the resuspension of particles from a surface and into a flow. We begin by explaining terms such as detachment, entrainment and re-entrainment, used commonly in aerosol science to describe the state of a particle with respect to the flow. The removal of a particle from a surface and into the flow depends on the relative magnitudes of several forces. Section 2.2 discusses the various adhesive forces that contribute to the attachment of a particle to the surface. Section 2.3 describes the counteracting aerodynamic forces that remove the particle from the surface as well as the theoretical models that aim to explain this process. Section 2.4 describes the various parameters and methods that are used to describe the flow of a fluid through a porous medium.

2.1 Introduction

Detachment refers to the process of separation of a microparticle adhering in static equilibrium to a surface by rolling, sliding or direct lift-off. Entrainment is the capture of the microparticle in the flow once it is detached. Resuspension or re-entrainment is the removal of a microparticle from a surface, where the microparticle was previously airborne and subsequently was deposited on the surface. The mechanics of resuspension depend primarily on the balance of two kinds of forces: adhesive forces that serve to keep the

particle attached to the surface, and counteracting aerodynamic removal forces. We describe these forces below in greater detail.

2.2 Process of Particle Adhesion

Particle adhesion forces are responsible for establishing contact and adhering particles to surfaces. Particle adhesion in solids is due to long-range forces, chemical interactions and very short-range forces.

Long-range attractive forces bring the particle to the surface and establish the adhesion contact area. These include van der Waals forces, electrostatic and magnetic forces. The establishment of the contact area is supported by chemical interactions like the building of solid and liquid bridges between particle and surface, resulting in capillary forces. The short-range forces include chemical and intermediate bonds such as hydrogen bonds.

2.2.1 Van der Waals Adhesion Force

Van der Waals forces predominate for particles below 50 _m in diameter, and electrostatic forces dominate for larger particles (Bowling 1988). The origin of van der Waals forces is quantum mechanical. For a non-polar atom, the average of its dipole moment is zero. However, at any instant there exists a finite dipole moment given by the instantaneous positions of the electrons about the nuclear protons. This instantaneous dipole generates an electric field that polarizes any nearby neutral atom, inducing a dipole moment in it (Israelachvili 1985; Israelachvili 1992; Friedlander 2000). This interaction

between the two dipoles gives rise to an instantaneous attractive force, as shown in Fig. 2.1.

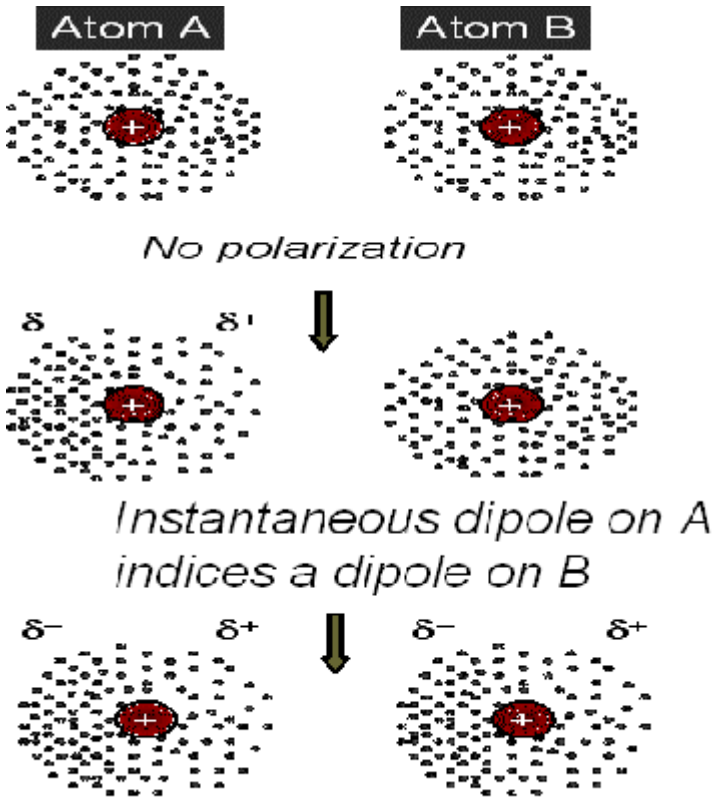

Fig. 2.1: Generation of Van der Waals attractive force between two non-polar atoms

The attractive van der Waals forces can be calculated using Hamaker's theory. The Hamaker theory integrates forces between individual atoms to determine the interaction between larger bodies. This method uses the Hamaker constant, A, which depends on the number density atoms in both the particles in contact and on the coefficient of van der Waals pair-wise interaction. The van der Waals interaction energy (Israelachvili 1992) between two spheres is given by

$$W_{sp-sp} = \frac{A(R_1 R_2)}{6D(R_1 R_2)} \tag{2.1}$$

where A is the Hamaker constant, R_1 and R_2 are the radii of the spheres that are close to each other and D is the separation between the spheres.

For a sphere-surface interaction, the interaction energy, $W_{sp\text{-}sf}$ is given by

$$W_{sp-sf} = \frac{A(R)}{6D} \tag{2.2}$$

where R is the radius of a sphere in close proximity of a surface.

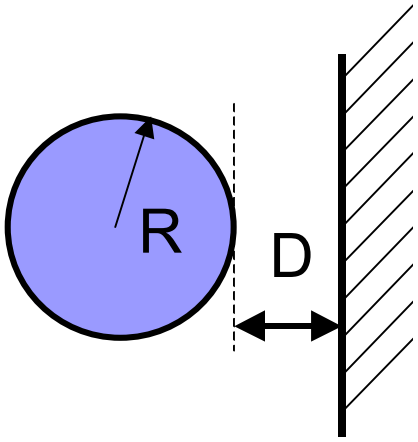

Fig. 2.2: Sphere-surface interaction

This approach has severe shortcomings because it extends a microscopic interaction to a macroscopic level. A more satisfactory macroscopic approach was developed by Lifshitz (Lifshitz 1956), who started directly from the bulk optical properties of the interacting bodies. In this approach, the material value is the Lifshitz-van der Waals

constant h, which is defined as the integral parts of the dielectric constants of the adhering particles. The van der Waals force, F_{vdw} for a spherical particle on a flat surface is given by

$$F_{vdw} = \frac{hR}{8\pi z^2} \tag{2.3}$$

where h is the Lifshitz-van der Waals constant, R is the particle radius and z is the atomic separation between the particle and the surface. The Lifshitz-van der Waals constant generally ranges from 0.6 eV for polymers to 9.0 eV for metals such as silver and gold. It depends on the combination of materials.

2.2.2 Electrostatic Force

The electrostatic adhesive force is the result of image and double layer forces. The image force is due to bulk excess charge present on the surface or particle, which produces Coulombic attraction. The image force is given by the equation

$$F_{image} = \frac{q^2}{4\pi\varepsilon_0\varepsilon l^2} \tag{2.4}$$

where q is the charge, ε is the dielectric constant of the medium between the particle and the surface, ε_0 is the permittivity of free space and l is distance between the charge centers and is approximately twice the radius of the particle.

The double layer force is due to the potential difference that develops between two materials in contact. Charge is transferred from one material to another until equilibrium is reached. In the equilibrium state, the current flow in both directions is the same. The

contact potential difference is in the range of 0 to 0.5 V. The distribution of the contact charge depends on the material. For example, in metals, only the surface has contact charges while in the case of insulators and semiconductors, these charges may extend 1 μm or more inside the material. The double layer force can be measured as

$$F_{dlf} = \frac{\pi \varepsilon_0 R U^2}{z} \tag{2.5}$$

where ε_0 is the permittivity of free space, R is the particle radius, U is the contact potential difference and z is the distance of separation between the two materials.

2.2.3 Gravitational Force

The attractive force on a particle due to gravity can be calculated based on the equation

$$F_{grav} = \frac{4}{3}\pi R^3 \rho g \tag{2.6}$$

where ρ is the density of the particle and g is the gravitational acceleration. The attraction due to gravity is insignificant in the case of particles smaller than 20 μm (Bowling 1988).

2.2.4 Other Forces that Contribute to Adhesion

Capillary condensation forces come into play due to humidity present in the surroundings. Condensation of water vapor takes place in the gap between bodies which are in contact. The capillary force is a function of the particle radius and the surface tension of the liquid in contact. It is given by

$$F_{cap} = 4\pi R \gamma \tag{2.7}$$

where R is the radius of the particle and γ is the liquid surface tension.

Studies indicate that there is almost no change in adhesion forces till about 30% relative humidity (Corn 1961; Stein 1965; Bhattacharya and Mittal 1978). However, at higher relative humidities, there is a rapid increase in adhesion forces. Water adsorbed between the surface and the particle increases the effective contact area and the corresponding pull-off force (Akiyama and Tanijiri 1989).

Van der Waals forces create tremendous pressure on particles and surfaces and lead to deformation. The amount of deformation depends on the hardness of the particle and the surface (Johnson, Kendall et al. 1971). The surface area of contact increases due to deformation, thereby increasing the adhesion force. The additional van der Waals force due to deformation is given by

$$F_{vdw\ deform} = \frac{h\rho^2}{8\pi z^3} \tag{2.8}$$

The effect of roughness of the surface on van der Waals force is dependent on the nature of the roughness. The roughness of real surfaces is a highly complex mix of height, curvature and distribution of asperities(Cheng, Dunn et al. 2003). In most cases, the roughness of a surface is characterized by an asperity radius, r and the distance between asperities, a. This is applicable in the case when the particle size, R, is considerably larger than the asperity size. This case is shown in Fig. 2.3a, where the roughness is fine and reduces the adhesion force. Fig. 2.3b, demonstrates a case where the size of the asperity is comparable to the particle size (Ranade 1987). A discussion on the effect of asperity size on the adhesion force is dealt with in section 2.4.

Fig 2.3a Surface with fine roughness

Fig. 2.3b Asperity size comparable to particle size

2.3 Particle Entrainment

The most common method of entrainment is by the application of aerodynamic or hydrodynamic forces. In the aerodynamic method, there are three modes of inceptive motion, namely, lift-off, rolling and sliding (Wang 1990; Mollinger, Nieuwstadt et al. 1992). Figure 2.4 demonstrates the balance of forces schematically.

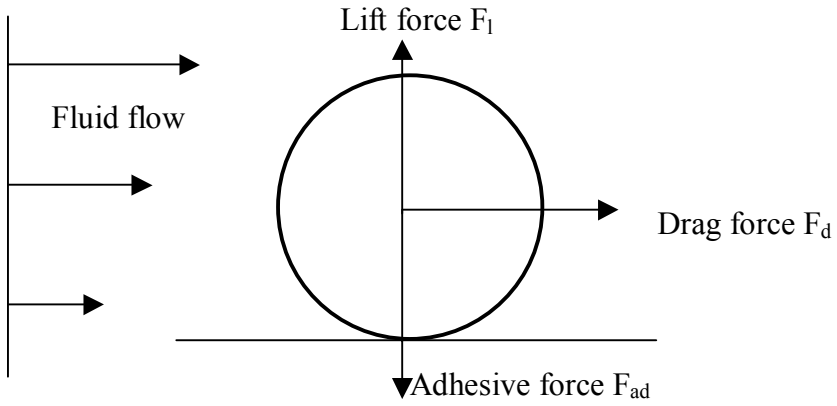

Fig. 2.4 Balance of forces

The particle gets directly lifted off the surface when the normal component of the applied aerodynamic force exceeds the adhesive force. The tangential component of the applied force overcomes the combined effect of frictional and adhesive force, resulting in sliding of the particle. The torque at the point of contact of the particle on the surface sets

the particle in a rolling motion (Denis J. Phares;Gregory T.. Smedley; Phares, Smedley et al. 2000).

The balance of forces resulting in particle resuspension can be explained using two basic models, namely the force balance (Cleaver and Yates 1973) and the energy balance models (Reeks 1988; Reeks 1988). The rock'n roll model(Reeks and Hall 2001) and aggregate wall-collision model (Adhiwidjaja, Matsusaka et al. 2000) are modifications to the energy balance model, in order to better estimate the resuspension rate.

2.3.1 Force Balance Model

Particles on a surface are held by very strong surface forces, which are a combination of physical interactions, chemical bonds and mechanical stresses. When the particles are subjected to very high turbulent flows, some particles get suspended due to the aerodynamic force (Ziskind, Fichman et al. 1995). The fluid flow counteracts the adhesion force. Particles get resuspended when aerodynamic forces exceed their surface counterparts (Cleaver and Yates 1973) . There is a strong dependence of the reentrainment rate on the frequency and intensity of the turbulent bursts (Wen, Kasper et al. 1989). Experiments using this model indicate that resuspension occurs in two regimes, namely the short-term regime (less than a few minutes) and the long-term regime. The short-term regime is characterized by a power law decay where the concentration of removed particles is proportional to t^{-a} (t is time and a is a function of flow rate and particle size). The concentration of particles in the long-term regime is proportional to $(1/t)\ e^{-t/T}$, where T is the decay constant (Wen and Kasper 1989; Jurcik and Wang 1991).

To better understand the force balance model, we first analyze the moment of forces on a single particle in contact with a surface as shown in Fig. 2.5.

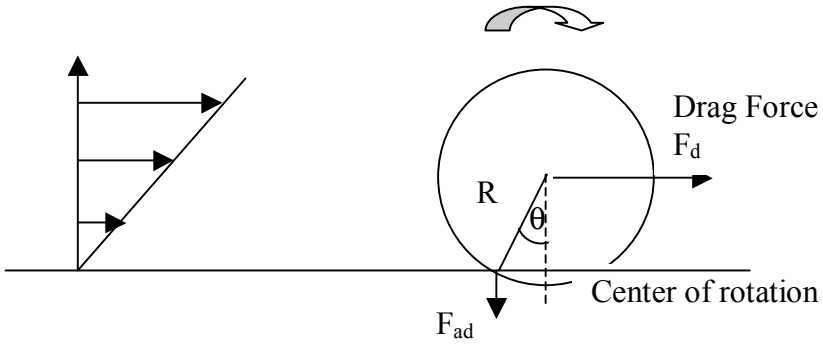

Fig. 2.5 Forces acting on a small agglomerate

With reference to Fig. 2.5, R is the particle radius, D_p the particle diameter, F_{ad} is the adhesive force (primarily van der Waals force) between the particle and the wall and θ is the contact angle of the aggregate with the wall. The moment of adhesion is given by

$$M_{ad} = F_{ad} D_p \sin \theta \tag{2.9}$$

The adhesive force F_{ad} consists primarily of van der Waals force, ignoring electrostatic, capillary and gravitational forces. Hence, The van der Waals force acting between the particle and the surface is given by

$$F_{ad} = \frac{AD_p z^{-2}}{12} \tag{2.10}$$

where A is the Hamaker constant and z is the separation gap between contact bodies. Substituting F_{ad} in equation for M_{ad}, we get

$$M_{ad} = \frac{AD_p^2 z^{-2} \sin\theta}{12} \tag{2.11}$$

The aerodynamic drag moment, M_d is given by (Matsusaka and Masuda 1996)

$$M_d = \frac{15\pi\tau_w D_p^3}{16} \tag{2.12}$$

where τ_w is the wall sheer stress caused by the airflow in a tube and is given by

$$\tau_w = 3.96\times10^{-2}\rho_f \nu_f^{\frac{1}{4}} D_t^{-\frac{1}{4}} u_{avg}^{-\frac{7}{4}} \tag{2.13}$$

where ρ_f is the density of air, ν_f is the kinematic viscosity, D_t is the diameter of the tube and u_{avg} is the average flow velocity. For resuspension to take place, the drag moments should be greater than the adhesion moment.

The force balance model of particle resuspension works well when the force of detachment is greater than the adhesion force. However, this model also has its limitations as it is unable to explain removal of nanometer sized particles where the removal force is less than the adhesion force. A modification of the force balance model tries to overcome this limitation by developing a model based on aggregation of nanoparticles.

2.3.1.1 Aggregates with Breaking Particle Collisions

This model is based on the agglomeration of very fine particles and their removal by breaking-particle wall collisions (Adhiwidjaja, Matsusaka et al. 2000) and we analyze the case by considering forces acting on an agglomerate of particles. Fine particles in aerosol flow form aggregates or a particle deposition layer (Theerachaisupakij, Matsusaka et al. 2003). A particle deposition layer is formed when the flow velocity is below a certain critical velocity. When the particle deposition and reentrainment rates are in equilibrium, the state of the deposition layer is controlled by the balance of the moments of

forces. As the flow velocity is increased gradually, the amount of the deposited particles decreases and the particle deposition layer changes into small aggregates. Collisions between particles have a significant effect on resuspension (Matsusaka and Masuda 1996). Once a few microparticles are detached, they move along the surface and impact other microparticles. This process of aggregation and detachment, provides enough momentum to the stationary microparticles to overcome their adhesion with the substrate (Gotoh, Karube et al. 1996; Ibrahim, Dunn et al. 2004).

From experiments it is observed that small nanometer-sized particles are present in the flow of resuspended particles. From this we infer that nanoparticles are removed even when they do not agglomerate, that is when the removal force does not exceed the surface adhesion. This conclusion can be explained using the energy balance model of detachment.

2.3.2 Energy Balance Model

The energy balance model is based on the understanding that entrainment occurs even though removal aerodynamic forces do not always exceed the surface adhesion forces. With every turbulent burst a particle accumulates kinetic energy and it gets resuspended when it overcomes the adhesive potential well. Particles in turbulent flow accumulate energy and finally get resuspended as shown in Figure 2.6.

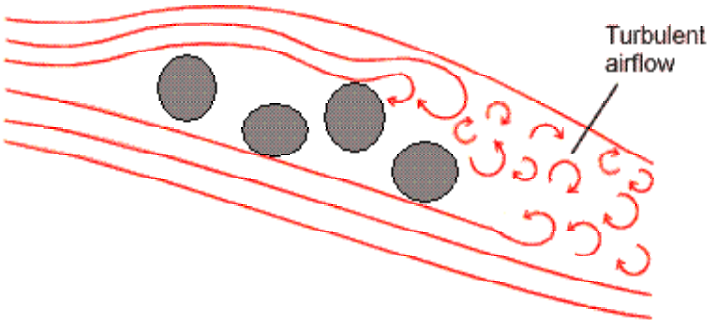

Fig. 2.6: Resuspension of particles by accumulation of energy in turbulent flow

The energy balance model introduces the concept of turbulent bursts or eddies, wherein the particles accumulate energy to overcome the adhesion potential well and get resuspended (Reeks 1988; Reeks 1988). It is based exclusively on lift/normal forces. Unfortunately, the energy balance model consistently underestimates the resuspension rate because it does not account for removal of particles due to sliding/rolling modes. It also assumes surfaces to be perfectly smooth and hence it does not consider the rocking of particles about surface asperities. The rock'n roll model overcomes these limitations of the energy balance model.

2.3.2.1 Rock'n Roll Model

The rock'n roll kinetic model considers the effect of drag (sliding) forces and also involves the rocking of a particle about an asperity in the contact zone (Ziskind, Fichman et al. 1997; Lazaridis, Drossinos et al. 1998; Reeks and Hall 2001). It considers the surface

to be rough and accounts for the variation in moments. The surface geometry of the rock'n roll model is shown in Fig. 2.7. As the particle oscillates about the asperity, the potential energy depends on the torque acting on the particle and the moment of inertia about the pivot. The analysis of the moments of a particle in contact with a rough surface depends on the height, distribution in space and the curvature of the asperities (Ziskind, Fichman et al. 1997).

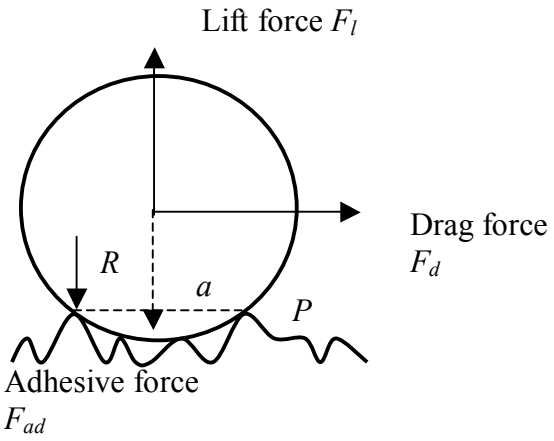

Fig. 2.7 Rock'n roll model to account for surface roughness

An asperity is characterized by its radius, r, and the distance between two asperities, a. We consider three cases of the rock'n roll model here with respect to one, two and three surface asperities.

When the size of a "large" particle (radius R) is significantly larger than the asperity ($R>>r$), the asperity acts like a small particle and the large particle plays the role of a flat surface (Lazaridis and Drossinos 1995). This is shown in Fig. 2.8a. This case is similar to that of a particle in contact with a smooth surface. In comparison to the adhesion force, F_{ad}

in Eq. 2.10 (where $D_p=2R$), we observe that in this case F_{ad} becomes smaller because it is calculated using the asperity radius and not the particle radius. Hence, F_{ad} is calculated using r instead of R. The contact of a particle with two surface asperities is of practical interest. The side view diagram of a particle on two surface asperities is shown in Fig. 2.8b. In this case, the rotation of the particle can occur in two directions. It can be along the line connecting the contact points, and it can also be along the line perpendicular to the previous one (Cheng, Dunn et al. 2002). These two directions of rotation are shown in Fig. 2.9a and b.

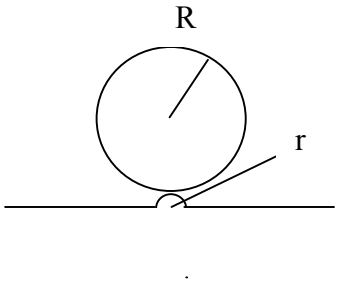

Fig. 2.8a Particle in contact with a single asperity (side view)

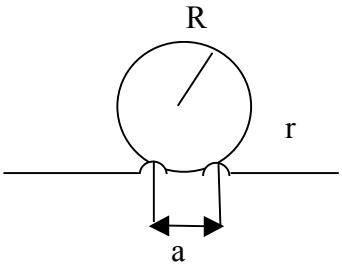

Fig 2.8b Particle in contact with two asperities (side view)

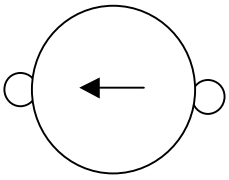

Fig. 2.9a Rotation along the line joining the asperities (top view)

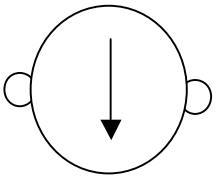

Fig. 2.9b Rotation along the line perpendicular to the line joining the asperities (top view)

The three asperity case is similar to the two asperity case. The first possibility is that the particle can move on the surface of an asperity. This will be similar to the case

shown in Fig. 2.9a. The second possibility is that the particle moves between the two asperities in which the direction of travel is perpendicular to the line joining the two asperities. This is similar to the case demonstrated in Fig. 2.9b. The two cases of the three asperity motion are shown in Fig. 2.10a and b.

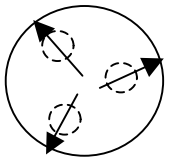

Fig. 2.10a Rotation of particle on surface asperity (top view)

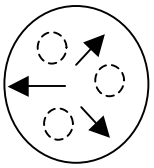

Fig. 2.10b Rotation of particle perpendicular to line joining two asperities (top view)

After gaining sufficient momentum, the particles lift-off/roll/slide on the surface, get detached and travel with the flow (Ibrahim, Dunn et al. 2003). If the flow of air is through a porous media, it is characterized by parameters like porosity, Reynolds number (Re), pressure difference, loss coefficient, interstitial velocity and volumetric flow rate.

2.4 Fluid Flow through Porous Media

In a porous medium, only a fraction of the cross section is available for fluid flow. The porosity, ε' of a medium is defined as the fraction of total volume of the medium that is occupied by void space. In defining the porosity of a medium we assume that all the void space is connected. The porosity of a bed composed of identical spherical bodies is independent of the grain diameter; it is a function of the mutual disposition of the grains, the angle θ (Idelchik and Fried 1986).

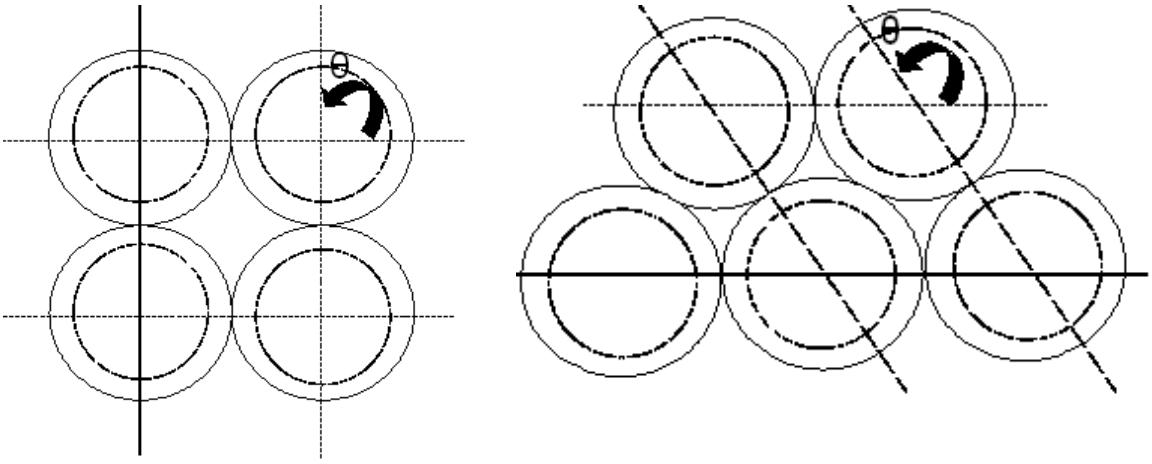

Fig. 2.11 Porosity varies between 60^0 and 90^0

Porosity for the extreme values of θ is given by:

$$\varepsilon' = 1 - \frac{\pi}{6(1-\cos\theta)\sqrt{1+2\cos\theta}} \tag{2.14}$$

The extreme values of θ are 60^0 and 90^0. The porosity of a bed of solid spheres, can vary between 0.25 to 0.47. Media made up of nonuniform sizes of grains have lesser porosity because smaller grains fill pores formed by larger grains. A characteristic feature of flow in porous media is a gradual transition from laminar to turbulent regime starting at low Reynolds numbers (Re) and extending over a wide range of values of Re (White 2003). The smooth transition in Re number is due to tortuosity of the pores, contractions, and expansions and surface roughness of the porous medium, which favors vortex formations and flow disturbances (Kaviany 1999). It is also due to the gradual propagation of turbulence from larger pores to smaller ones associated with the size distribution of

pores in the medium. Figure 2.12 shows the flow of fluid through a porous medium composed of grains on non-uniform size.

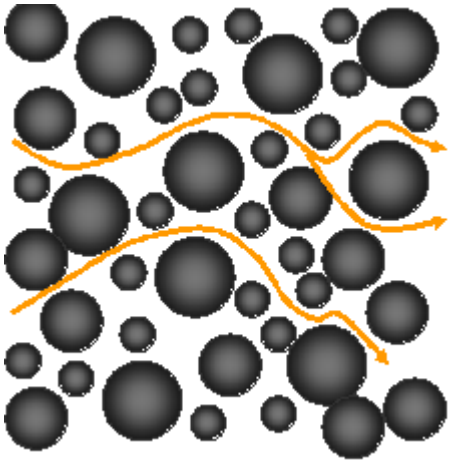

Fig. 2.12 Flow of fluid through porous medium composed of non-uniform grain size

The flow of a fluid through a porous medium or packed bed involves several parameters, namely pressure loss, bed porosity and length, volumetric flow rate, interstitial velocity and the Reynolds number depending on whether the flow is in the laminar or turbulent regime. The flow parameters of a packed bed can be determined using two methods – Darcy and Idelchik methods.

2.4.1 Darcy's Method

Darcy's method is based on Darcy's law, which states that for a steady-state unidirectional flow in a uniform medium, the relation between the flow rate and the applied pressure difference is given by

$$u = -\frac{K}{\mu}\frac{\partial P}{\partial x} \tag{2.15}$$

where $\frac{\partial P}{\partial x}$ is the pressure gradient in the flow direction, μ is the viscosity of the fluid, K is the hydraulic conductivity of the medium (it is independent of the nature of the fluid) and u is the flow rate. The hydraulic conductivity, K is a function of the size and distribution of the pores in the medium. It is essentially a measure of the size, orientation and connectedness of the pores. Darcy's method to calculate the flow parameters is valid for only laminar flow. Further, it is necessary to know the permeability k of the medium.

2.4.2 Idelchik Method

The Idelchik method is valid for laminar or turbulent flow through a bed. Any value of porosity may be used. Another advantage is that, using the Idelchik method, permeability can be back-calculated for use in Darcy's method.

To calculate flow parameters using Idelchik's method, we consider a column with area A_{up}, bed length l, packed with grains of diameter d of total weight, w and density, ρ. The bed length, column cross-sectional area A_{up}, area of bed A_{bed} (column cross-sectional area minus area of grains), the volumetric flow rate (Q), fluid density (ρ), fluid viscosity (μ) and bed porosity ε' are the parameters that we need to know. The values that we can measure are interstitial/pore velocity (V_{bed}), Reynolds number (Re), pressure difference (ΔP), bed permeability k and the minor loss coefficient (K_m) of the bed.

The method to calculate the flow parameters is as follows. The porosity of the bed ε' is given by Eq. 2.14. For a bed of spherical particles, the extreme values for θ are in the

range of 60^0-90^0. From the values of volumetric flow rate Q and column cross-sectional area A_{up}, we determine the upstream velocity V_{up} using the equation

$$V_{up} = \frac{Q}{A_{up}} \tag{2.17}$$

Using the assumption that the input volumetric flow rate is equal to the output flow rate, we get the relation

$$Q = V_{up} A_{up} = V_{bed} A_{bed} \tag{2.18}$$

From the above relation we can determine the value of the interstitial velocity or the pore velocity, V_{bed}.

From the two extreme values of porosity, we can determine the range of Re for the flow as given below

$$\mathrm{Re} = \frac{DV_s\rho}{(1-\varepsilon')\mu} \tag{2.19}$$

The pressure gradient across the bed is given by the equation

$$\Delta P = \frac{1.53L}{D\varepsilon'^{4.2}\left(\frac{30}{\mathrm{Re}} + \frac{3}{\mathrm{Re}^{0.7}} + 0.3\right)} \times \frac{\rho V_{up}^{\ 2}}{2} \tag{2.20}$$

The minor loss coefficient is given by the equation

$$K_n = \frac{2\Delta P}{\rho V_{up}^{\ 2}} \tag{2.21}$$

The permeability of the bed can be back calculated for use in Darcy's method using the relation

$$k = \frac{V_{up}\mu l}{\Delta P} \tag{2.22}$$

In Chapter 5, the Idelchik method is used to determine the flow parameters of the bed. It also provides the permeability of the bed for use in the Darcy's method.

2.5 Summary

This chapter covered the important aspects that affect the resuspension of particles from a bed of substrate particles. We discussed the forces that affect the attachment and detachment of particles, especially the ones that become prominent for sub-micron particles. Different models and their modifications try to explain the results from experiments. The characteristics and important parameters of particles suspended in porous media were discussed. Two alternate methods, the Darcy method and the Idelchik method explain the calculation of the flow parameters in laminar and turbulent flow in porous media.

CHAPTER 3 Experimental Setup

3.1 Introduction

This chapter describes the experimental setup, materials and method used to investigate the detachment of nanoparticles from the surface of micron-sized substrate spheres under the influence of air flow. A known size and quantity of micro and nanospheres were packed in a tube. All flow parameters were controlled to study the effect of particle size on resuspension. Section 3.2 provides information about the experimental setup and the instrumentation. Material specifications and the sample preparation are discussed in Section 3.3. Section 3.4 describes the experimental technique and the procedure used to set the control parameters. Finally, Section 3.5 explains how a set of controlled experiments is carried out to ensure consistent and repeatable results.

3.2 Experimental Setup

Figure 3.1 shows a schematic of the experimental setup. The setup consists of a gas filter, a mass flow controller (MFC), a mass flow meter (MFM), a pressure transducer, a humidity sensor, a steel capillary tube where the mixture of nanoparticles and substrate beads is held, particle filters, condensation particle counter (CPC) and a computer for data acquisition (PC).

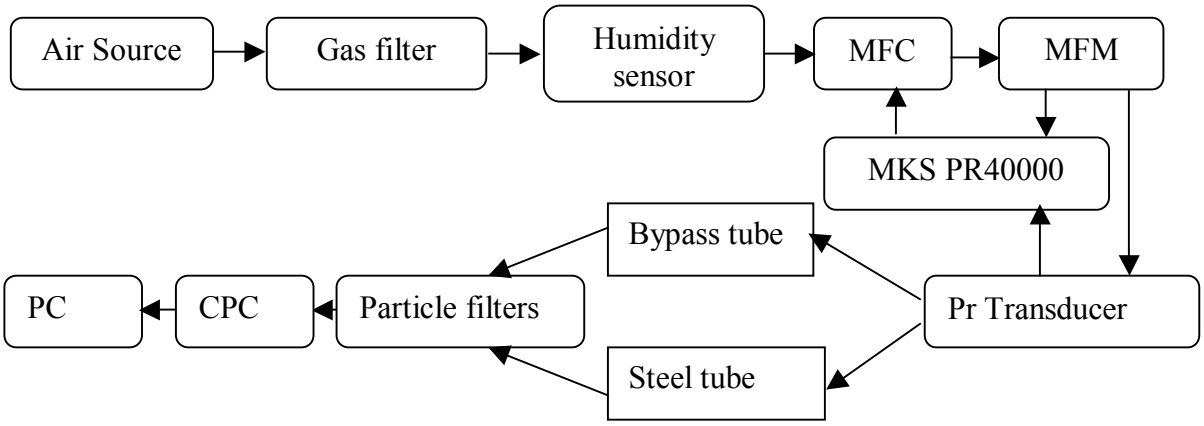

Figure 3.1 Schematic block diagram of the experimental setup

The air source in the setup is connected to a series of gas filters. The gas filter is a TSI 3074B, and it removes particles, water and oil droplets. The filter contains activated carbon pellets which remove even trace amounts of oil. The final stage of the filter contains a membrane dryer which removes water vapors in the gas. Before the start of the experiment, the inlet air is cleaned to a maximum of 0.01 particles per cm^3. The mass flow controller MKS 1559 and the mass flow meter MKS 558 are used to control the flow rate of the air that enters the tube. The mass flow meter and the controller have a full scan range of 100 Lpm, an accuracy of ± 1% and a resolution of 0.1% of full scale. The MKS PR 4000 controls the volumetric flow rate at the tube inlet. The inlet pressure and the volumetric flow rate are read by the MKS PR 4000. Figure 3.2 shows a photograph of the setup.

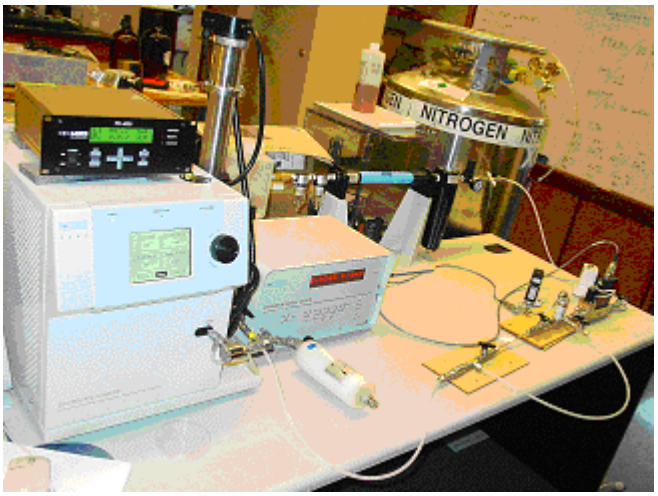

Figure 3.2: Picture of the experimental setup

The steel tube is filled with micrometer-size particles which act as the substrate particles. The tube is 1.75 mm O.D. × 160 mm in length, with an internal bore of 1.6 mm. On the surface of the substrate are the nanometer-size particles. The method for preparing the mixture of micrometer and nanometer sized particles is described in Section 3.3.4. There is a bypass tube in parallel with the sample tube through which the filtered air flows before and after the experiment at the set flow rate. A valve along with a 3-way fitting regulates the air flow between the sample tube and the bypass tube. A similar valve at the end of the parallel tube combination directs the flow into a set of particle filters. A set of swagelok particle screens are placed after the sample tube (40 μm and 20 μm). They prevent the larger micron sized spheres from entering the particle counter.

The TSI 3022A condensation particle counter (CPC) is used to measure the concentration of nano particles. It can detect particles in the size range from 15nm – 1μm. At 15nm, the CPC detects 90% of the particles. The detectable concentration of the

particles is from 0 to 9.99×10^6 particles/cm^3. The aerosol enters the CPC at a fixed flow rate of 25 cm^3/s. Out of this, 5 cm^3/s of the flow is branched toward the sensor of the CPC for counting of the particles. Aerosol enters the saturator tube of the CPC and passes through a wick which is soaked in *n*-butanol. The liquid evaporates and saturates the aerosol stream with vapor. This passes through the condenser tube, becomes supersaturated, and condenses on the particle to form larger detectable droplets. The particles are detected by the optical detector by scattering of laser light. The concentration of particles is detected by the CPC and is recorded by the computer.

3.3 Materials and Sample Preparation

3.3.1 Introduction

The steel tube is filled with a known amount and fixed composition of a mixture of micrometer (Missouri Scientific) and nanometer (Bangs Laboratories) sized silica beads (a packed bed). Three different sizes of micrometer and nanometer sized silica beads are used to obtain 9 combinations of substrate-particle beds. The specification and properties of the nano and micron sized substrate particles are explained in Section 3.3.2 and 3.3.3. Various tools such as the scanning electron microscope (SEM), the atomic force microscope (AFM), optical and confocal microscopes, as well as potential analysis and sizing methods are used to understand and measure the surface properties and the size distributions. Finally, we discuss the procedure for sample preparation.

3.3.2 Properties of the substrate particles

The micrometer-sized substrate beads are composed mainly of silica with small amounts of oxides of aluminium, calcium, magnesium, sodium and iron. The chemical composition (by weight) is listed in Table 3.1.

Table 3.1 Chemical composition (by weight) of micron-sized substrate beads

Silica	65~75%
Aluminium oxide	0~5%
Calcium oxide	6~15%
Magnisium oxide	1~5%
Sodium oxide	10~20%
Iron Oxide	<0.8%

The physical properties of the microspheres are listed in Table 3.2.

Table 3.2 Physical properties of the silica microspheres

Bulk density of dry beads	1.3 g/cm^3
pH in water at 25^0C	7.8
Refractive index	1.5
Hamaker constant	$8.5\times10^{-20}J$
Specific gravity	2.5 g/cm^3
Softening temperature	650^0C
Coefficient of thermal expansion	$90\times10^{-7}/^0C$
Compression strength	29 kg/mm^2

The silica microspheres are selected in 3 size ranges. The ranges are 250-350μm, 350-500 μm and 590-840μm. They were inspected under an optical microscope and an image of the 250-350 μm sized beads is shown in Fig. 3.3. The surface of the silica microspheres appears “smooth” at this magnification.

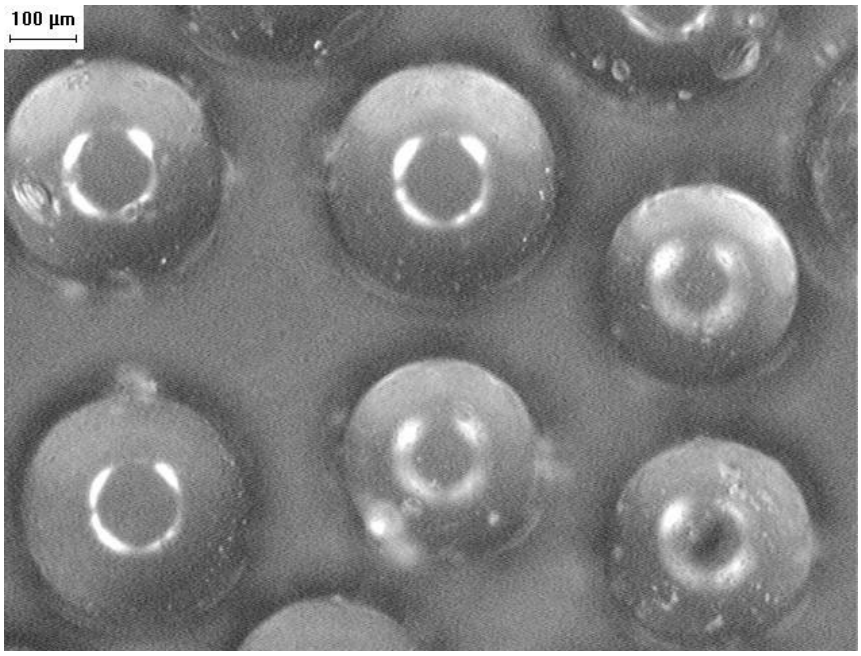

Figure 3.3: Optical microscope image of the glass substrate

From the literature review, we understand that the size and rms roughness of the microspheres decide the contact area between the microspheres and nanospheres and hence, the surface adhesion force.

We use an atomic force microscope (AFM) to determine the surface roughness of the substrate beads. The AFM measurements also provide information regarding the adhesive force.

The roughness measurements were carried out by measuring the root mean square (rms) height of several 12×12 μm^2 areas on the surface of the bead. This measurement was repeated for several beads of the same size range. There was variation based on the region selected, the area scanned and the bead. However, the average of all the measurements for

a specific size range gave an idea of the rms roughness. An AFM roughness plot is shown in Fig. 3.4.

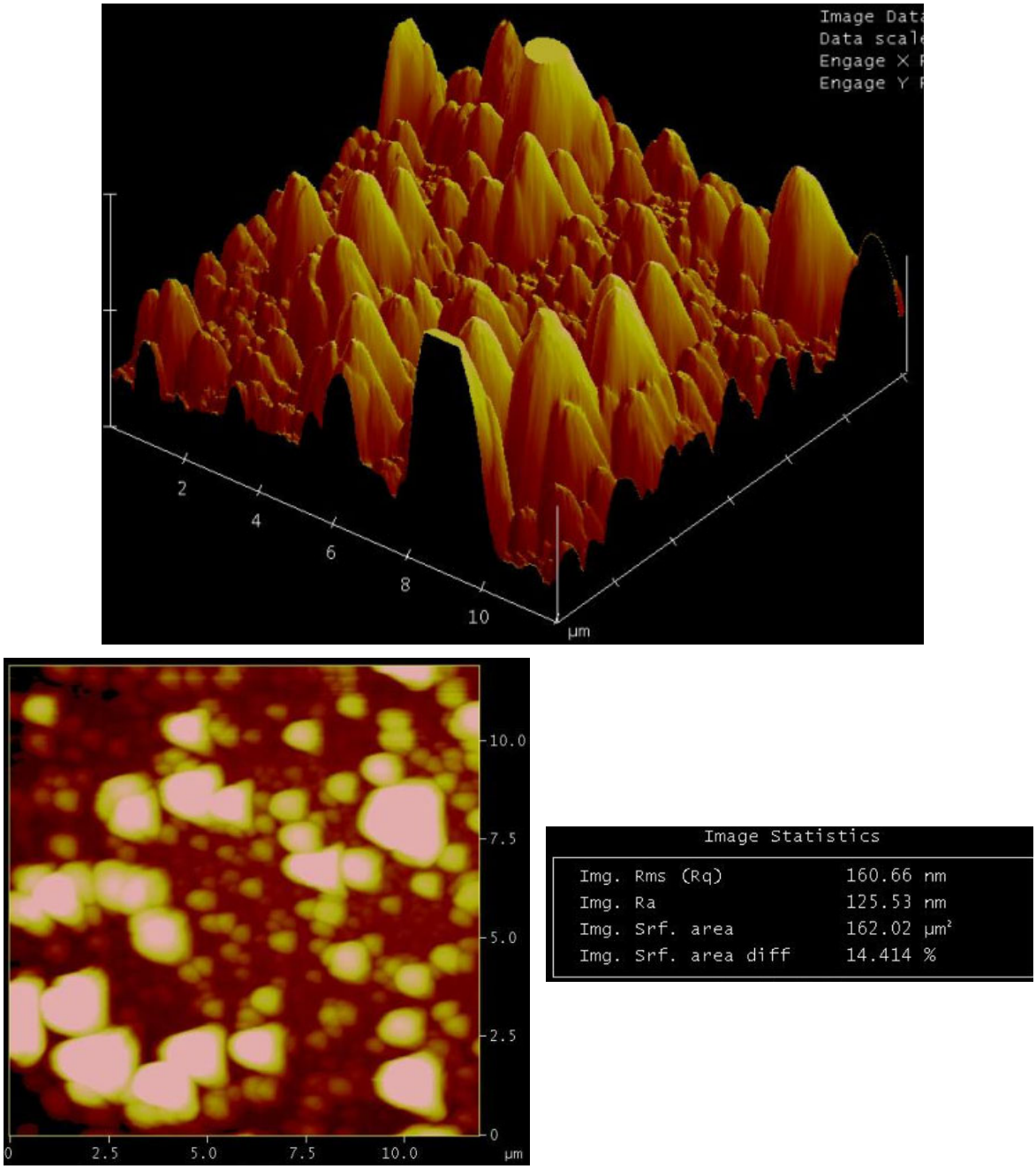

Figure 3.4: Roughness profile of 590-840 µm substrate particle

The rms height of the different sizes of silica microspheres is given Table 3.3.

Table 3.3 Rms roughness of silica microspheres

Size (μm)	Rms height of surface asperity (nm)
590-840	123
350-500	100
250-350	155

We have a size range of microspheres from the manufacturer. To determine the mean size of each range, the Horiba camsizer was used. The beads were also measured for their sphericity and symmetry. The values of the camsizer measurements are tabulated in Table 3.4.

Table 3.4 Mean size, sphericity and symmetry of substrate particles

Size range (μm)	Median size (μm)	Sphericity	Symmetry
590-840	648	0.85	0.92
350-500	360	0.87	0.89
250-350	272	0.80	0.85

From Table 3.4, we understand that the microspheres are more symmetrical than spherical. This is further validated by SEM microimages presented in Section 3.3.3.

3.3.3 Properties of the entrained particles

For the experiment, the nanospheres are deposited on the surface of the micron-sized silica beads, as shown in the SEM microimage (Fig. 3.5). A higher magnification image of the nanospheres is shown in Fig. 3.6. Also, as discussed in Section 3.3.2 (the Horiba camsizer measurements), the microspheres appear to be more symmetrical than spherical. This is apparent from Fig. 3.7.

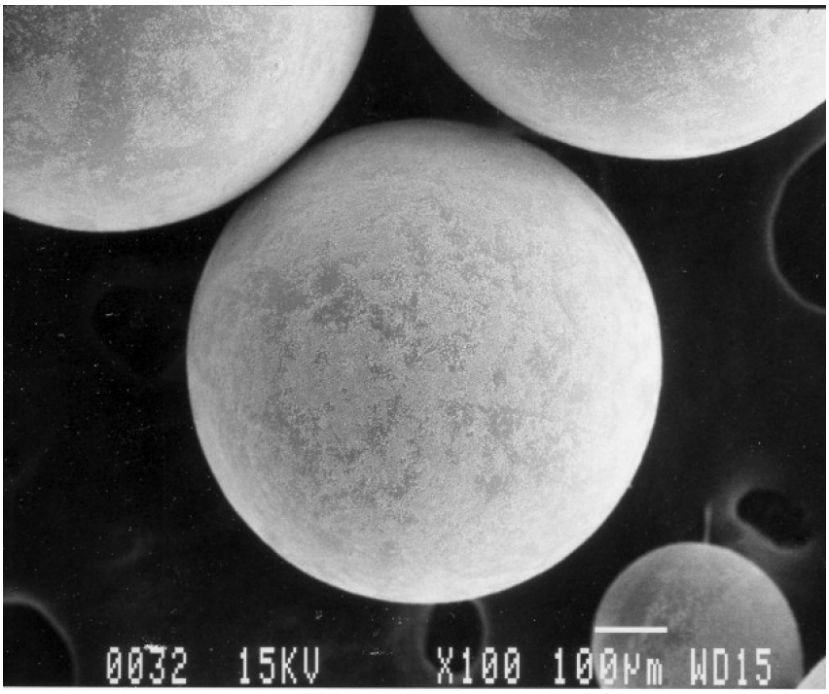

Fig. 3.5 Nanospheres on the surface of silica microspheres

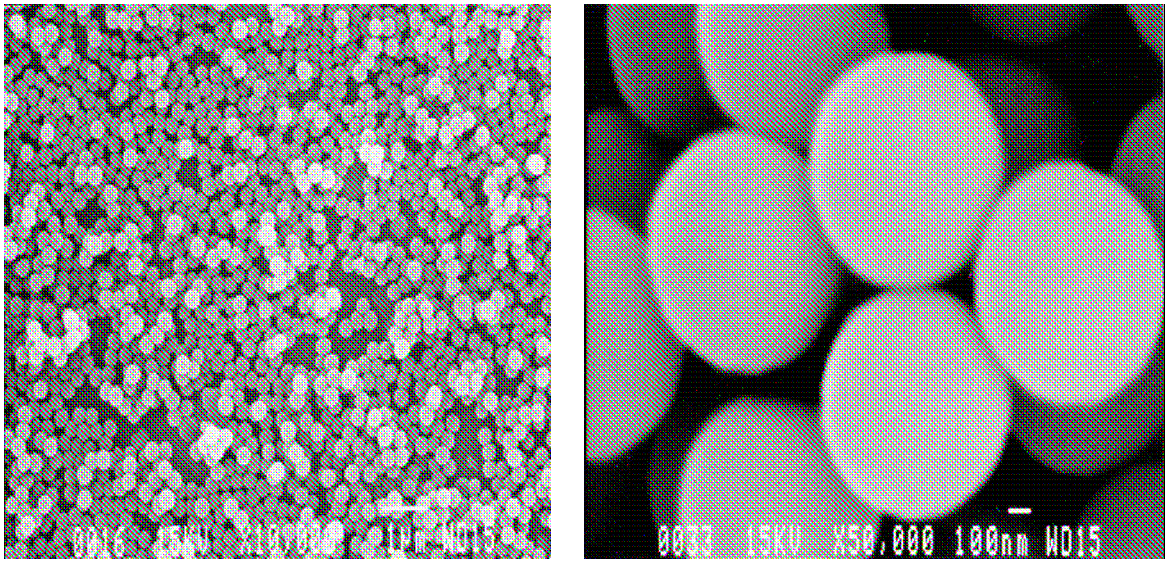

Fig. 3.6 Closer view of the silica nanospheres

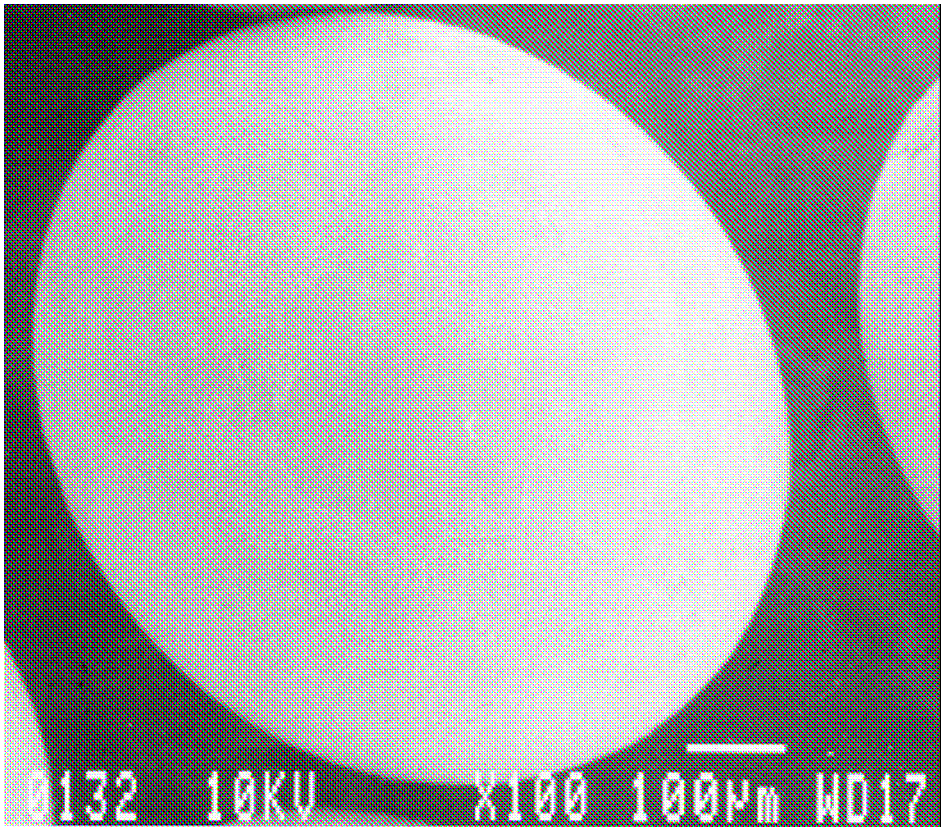

Fig. 3.7 Microimage showing higher symmetry than sphericity of microspheres (nanospheres are present on the surface)

The monosized nanospheres (Bangs Laboratories) lie within a very narrow size range. This is necessary in order to limit the range of surface adhesion forces (Phares 2000). Further, the particles absorb moisture on exposure to air and tend to agglomerate. This tendency is retarded by using particles that have a surface charge and repel each other. Zeta potential is a useful and important indicator of this surface charge and determines the stability of colloidal suspension or emulsion. The measurement of zeta potential can predict the aggregation behavior of particles. The size and zeta potential measurements of the nanospheres were conducted using the ZetaPlus (Brookhaven) particle size analyzer.

The potential was measured by making a suspension of the nanospheres in de-ionized water (pH 6.825). A snapshot of a sample measurement is shown in Fig. 3.8. The size and surface potential measurements of the nanospheres are tabulated in Table 3.5 and a snapshot is shown in Fig. 3.9.

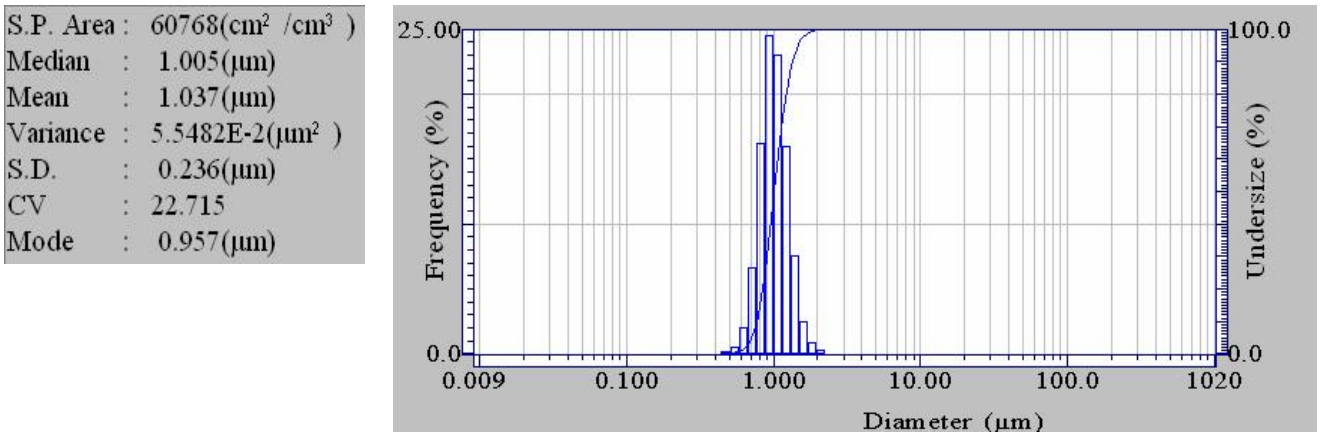

Fig. 3.8 Snapshot of the particle size measurements of the nanospheres

Table 3.5 Median size and zeta potential measurements of the nanospheres

Size (nm)	Measured size (nm)	Zeta potential
970	1037	-16.27
570	575	-35.88
330	340	-16.27

Run	Mobility	Zeta Potential (mV)
1	-2.75	-35.26
2	-2.57	-32.84
3	-2.58	-32.98
4	-3.04	-38.92
5	-2.88	-36.81
Mean	-2.76	-35.36
Std. Error	0.09	1.16
Combined	-2.76	-35.34

Fig 3.9 Snapshot of the zeta potential measurements of the nanospheres

3.3.4 Sample preparation

The nanoparticles are stored at 3-4^{0}C to prevent agglomeration. The nanoparticles are mixed with the substrate particle in a series of steps as described here. First, 0.25% (by weight) of nanoparticles is mixed with the silica microspheres to make a mixture. The total weight of the mixture is noted. The mixture is then put in a glass bottle, which is placed inside a bin tumbler. The inner walls of the bin tumbler should be padded sufficiently to prevent jerking while mixing. The bin tumbler is rotated at 40 rpm for a period of 7 days. It is necessary that the mixture be used in the experiment immediately to reduce residence time. It should be discarded after a period of 2-3 days. It is necessary to take care that the mixture does not undergo any harsh mechanical agitation or jerking. Such agitation can cause the nanoparticles to break or cause a change in the distribution on the substrate surface. The microimages in Fig. 3.9 show the effect of harsh mechanical agitation

observed in this work. As can be seen, the nanoparticles are crushed and removed from the substrate surface.

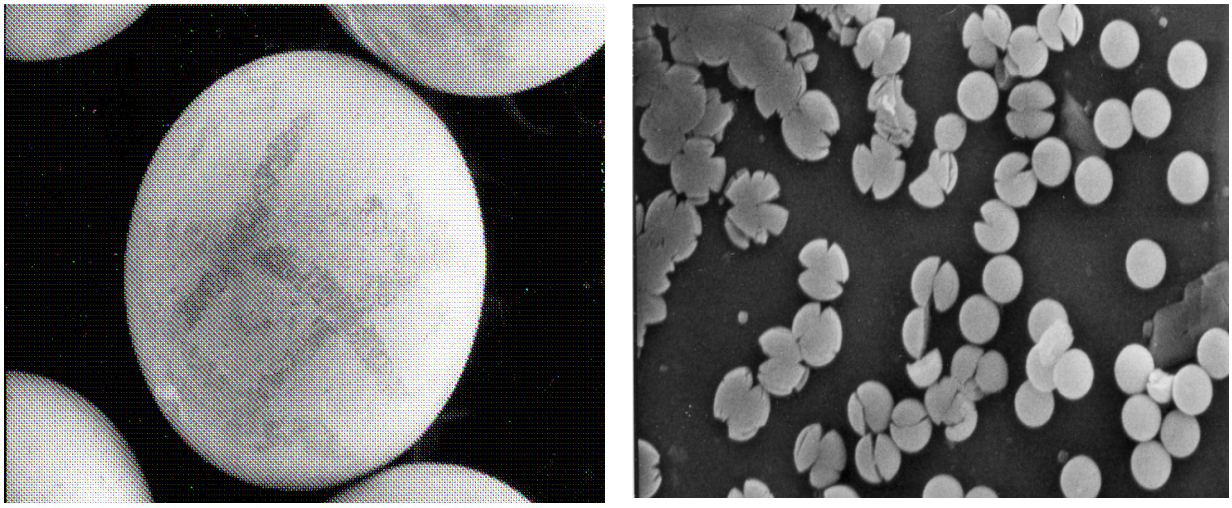

Fig. 3.10 Effects of mechanical agitation on the mixture

The steel tubes need to be thoroughly cleaned and dried before the experiment. The tubes are first sonicated in a bath of soapy solution for 24 hours. Then, they are rinsed in acetone and sonicated in an ultrasound bath containing acetone for another 24 hours. This is followed by rinsing and sonication in propanol and de-ionized water for a period of 24 hours each. The clean steel tubes are dried in a jet of filtered air and stored in clean glass jars. Before the start of the experiment they are dried again in a jet of filtered air. Then a tube is placed in the experimental setup (without any mixture inside) and filtered air is passed through it. The particle counter should read within a range of 0.05-0.01 particles per cm^3. This is done to ensure that no particles are present inside the tube before the sample is added to it. If the measured value does not lie within the permissible particle count range, a different steel tube should be used.

In the silica experiments, the sample is filled in the tube and the interstitial velocity is maintained at a fixed value. The Idelchik method outlined in section 2.4.2 is followed to determine the flow parameters. The volumetric flow rate was varied along with the size of the substrate particles to keep the interstitial velocity constant. A sample calculation for 250-350 μm sized substrate particles is described here.

The maximum possible volumetric flow rate for the 250-350 μm sized particles is Q = 4.9 l/min. The range of porosity for extreme values of mutual disposition of 60^0-90^0 is calculated using Eq. 2.14. The values of porosity are between 0.26 and 0.47. From the dimensions of the steel tube, we determine the column cross-sectional area, $A_{up} = 2.01\times10^{-6}$ m^2. The upstream velocity, V_{up} is calculated from Eq. 2.17. Using the relation in Eq. 2.18, we get the interstitial velocity V_{bed} to be 101 m/s. From this value of interstitial velocity, we determine the Re number for this range of substrate using Eq. 2.19. The pressure gradient, loss coefficient and permeability are determined from Eqs. 2.20, 2.21 and 2.22. For a different size of substrate particles, the value of the volumetric flow rate is adjusted so that the interstitial velocity in all the trials is set at 101 m/s. We run the experiment at its limit so that it results in maximum entrainment.

3.4 Experimental procedure

This section describes the experimental procedure for the measurement of detachment fractions. The steel tubes (1.75 mm O.D. x 160mm length) with an internal bore of 1.6 mm are weighed using a sensitive balance before the experiment. Humidity and

temperature are measured. We note that humidity should be below 50%. Humidity higher than this value can affect particle count.

Then the tube it is filled with a mixture of substrate and sub-micron particles, and is weighed again. In all the experiments the interstitial velocity is maintained at 101 m/s. The flow rate is set differently depending on the size of the substrate particles. Filtered air is allowed to pass through the bypass tube at the required flowrate until the count in the particle counter drops to 0.01 particles/ cm^3. The sample tube is then placed in the experimental setup. The flow of air is now allowed into the steel tube while stopping it through the bypass.

While the experiment is running, the flow rate is monitored to ensure that the actual flow rate is the same as the set flow rate. The experiment is allowed to run for an hour. On completion of the experiment the air is shut off in the sample path and allowed to flow through the bypass. The weight of the sample on completion of the experiment and any spill that may have occurred are noted.

3.5 Closure

This chapter described the experimental setup, sample preparation and the experimental procedure for the measurement of detachment fractions. We present results from the measurements in Chapters 4 and 5.

CHAPTER 4 Ground work – Carbon study

Prior to conducting the controlled experiments using silica particles, we conducted a series of experiments using charred carbon particles and in this chapter, we present results from experiments on the resuspension using the carbon particles. In this case, the nanoparticles are on the surface of micrometer-size charred carbon substrate particles.

However, the carbon particles used in this study suffered from two drawbacks that limit controlled resuspension experiments. Firstly, their distribution in size varied across 10^4 orders of magnitude, complicating any studies on size effects. Secondly, their shapes were irregular with very high surface asperities, which introduced inaccuracies in particle counting based on weight. Despite these limitations, the particles provide a starting point for studying the interactions of micrometer-size substrate particles and nanoparticles and this study serves as the foundation for the more controlled experiments on silica particles that are described in the next chapter. We describe the objectives of the experiments in Section 4.1. The properties of the carbon particles used in the experiments are given in Section 4.2. This is followed by a description of the experimental procedure. The results of the carbon study are discusses in section 4.4 and 4.5. Section 4.6 discusses the limitations of the carbon study.

4.1 Objectives of the carbon study

The main objective of the carbon study is to identify factors that affect the resuspension process as well as those that introduce randomness in the measurements. In particular, we study the effect of flow rate on the count and size of resuspended particles. We test the validity of the three models of resuspension of particles: force balance, energy balance, and aggregates with breaking particle collisions. These models have been discussed in detail in Chapter 2. Finally, we aim to identify the factors that introduce randomness and complications in understanding the effect of size (of the micro- and nanoparticles) on the resuspension process.

4.2 Properties of the carbon particles

The carbon mixture contains micron-sized carbon particles on the surface of which are nano-sized charred carbon particles. The mixture consists of primarily carbon with oxides of several metals and non-metals.

We found the carbon particles to have a very broad range of size. The Malvern Mastersizer 200 measured particles in the range from 300 nm to 1200μm (Fig. 4.1). The size is divided into two regions, one in the micrometer range for the substrate particles and the other in nanometer range for the nanoparticles on its surface.

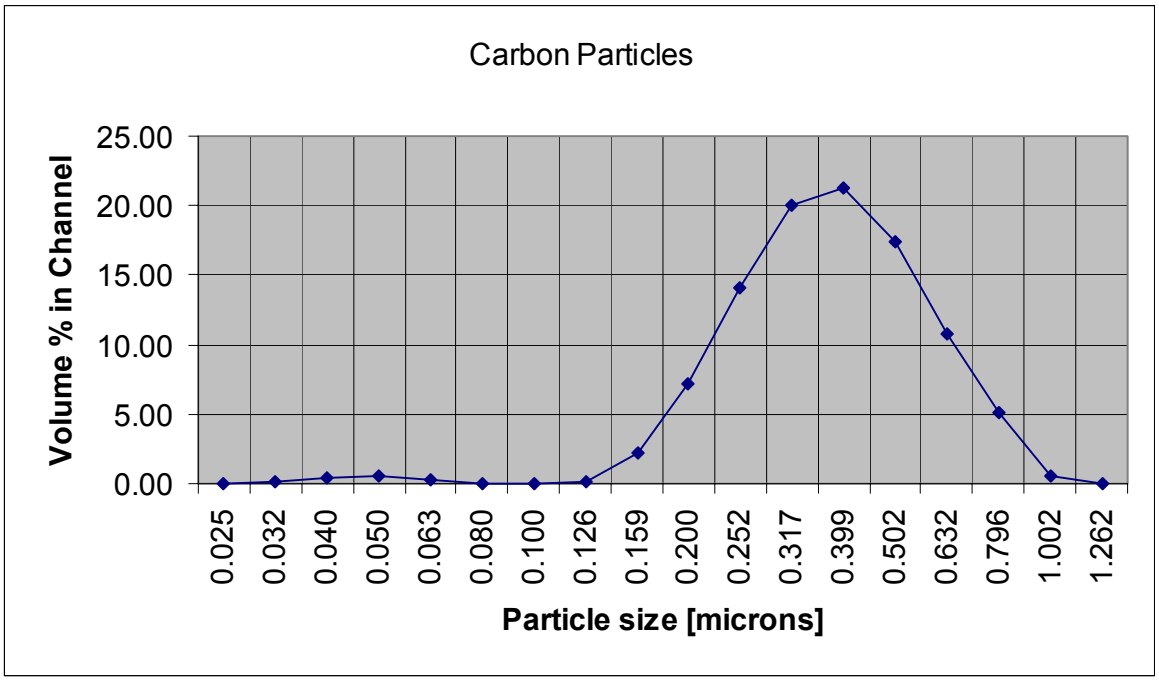

Fig. 4.1 Size distribution of carbon particles

We also found the carbon particles to be very irregular in shape. This is seen from Fig. 4.2, which shows an image of an angular carbon particle obtained using a Zeiss confocal microscope. The surface of the carbon particles is highly rough with asperities as high as 140 μm. A typical cross-sectional profile of the surface is shown in Fig. 4.3.

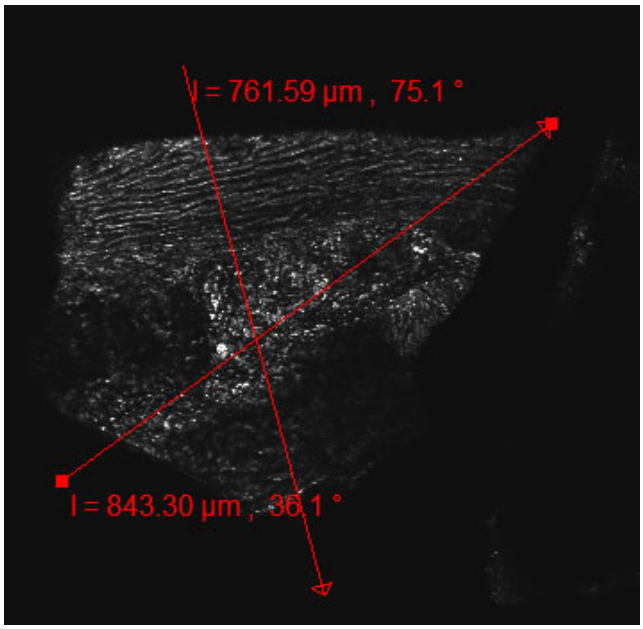

Fig. 4.2 Shape of a carbon substrate viewed under the confocal microscope

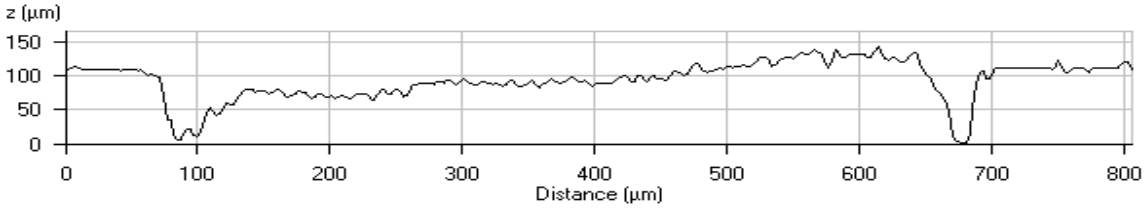

Fig. 4.3 cross-sectional surface profile of a carbon particle

4.3 Overview of the experimental procedure

The experimental procedure for the carbon study is similar to that for the silica beads, described in Chapter 3. Before the start of the experiment, the steel tubes are cleaned as outlined in Section 3.3.4. The tube is first weighed and then filled with the carbon mixture. The tube is weighed again and then placed in the experimental setup. The flow rate is set and air is allowed to pass through the bypass tube. Then, the flow into the sample tube is turned on while it is shut through the bypass. The particles resuspended from the sample

enter the condensation particle counter at a set flow rate of 1.3 l/min. The experiment is run for an hour. At the end of the experiment the tube is weighed again. The experiment is repeated several times for each flow rate. The experiment was conducted at seven different flow rates.

4.4 Experimental results

In the carbon experiments the volumetric flow rate was increased from 1.0 to 2.9 l/min over seven steps. Measurements were repeated 4 times at each flow rate. At the end of each run, the total particle count and the weight of resuspended particles were noted. The particle count that is read from the counter is the number density of particles. The flow rate that enters the sensor chamber of the counter is 0.3 l/min. The particle density has to be converted to particle count. The calculation for the particle count is given below.

Flow rate at the entry point of the sample = f_1 l/min

Weight of the tube (with the carbon mixture) before the experiment = w_1 mg

Weight of the tube after the experiment = w_2 mg

Weight of resuspended particles = $w_1 - w_2$ mg

Particle number density = n_1 particles/cm^3

Flow rate at which the released particles enter the sensor chamber = 0.3 l/min

= 5 cm^3/s

The time step at which each measurement is being taken = 0.1 s

Volume measured in the sensor at each time step = 5 cm^3/s× 0.1 s = 0.5 cm^3

Hence, the total particle count = $n = n_1 \times 0.5$

Average weight of typical nanoparticle = $w_{avg} = (w_1 - w_2)/n$ (4.1)

Particle count = $n = n_1 \times 0.5$ (4.2)

In the next two subsections, we discuss the observed effect of flow rate on the total count and size of resuspended particles.

4.4.1 Effect of flowrate on resuspended particle count

Table 4.1 tabulates the raw count (as a percentage) and the corrected count of the resuspended particles as a function of the flow rate. Figure 4.4 shows a plot of the same data. As seen from the plot, the total particle count increases and then plateaus off (a flow rate of 2.9 l/m is the limit of the experiment). A statistical analysis of the data shows that the total particle count increases significantly ($\alpha = 0.95$, p-value <0.0076) with increase in flow rate. The dashed blue line is a quadratic fit through the data points. We find the empirical relation to be

$$n(10^6) = -15 f_1^2 + 85 f_1 - 60 \quad (4.3)$$

where n is the particle count in units of 10^6 and f_1 is the flow rate in l/min.

Table 4.1 Variation in total particle count with flowrate

Flowrate (l/min)	% Resuspended particles (x2)	Particle count
1.0	0.95	1.75×10^7
1.3	1.02	1.20×10^7
1.5	4.52	3.35×10^7
1.8	2.10	4.30×10^7
2.1	1.20	0.55×10^8
2.4	1.42	0.60×10^8
2.9	1.81	0.55×10^8

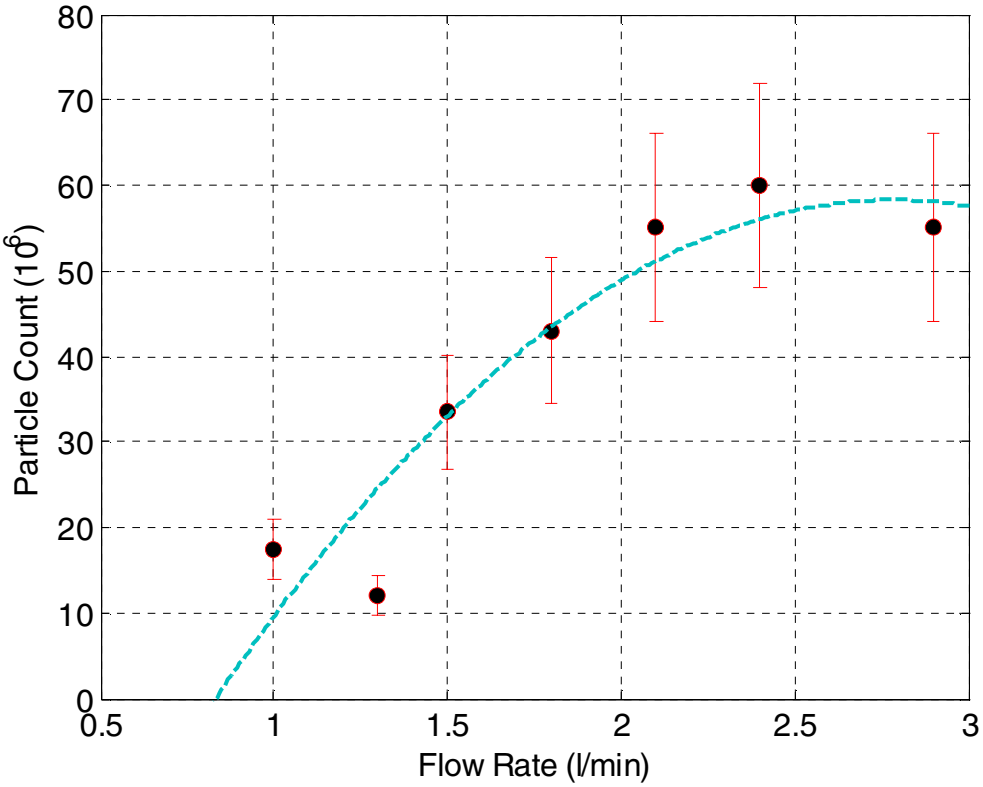

Fig. 4.4 Graph depicting the increase in particle count with respect to flow rate.

4.4.2 Effect of flow rate on the size of the resuspended particles

From the flow experiments, we get the weight and count of the resuspended particles. The average weight of a nanoparticle can be determined from Eq. 4.1. Since the exact composition of the carbon mixture is not known, we assume a particle with a lower average weight to be a smaller particle. With this assumption, we now compare the effect of flow rate on the average weight of the resuspended nanoparticle. Further, from this comparison we can obtain an understanding of the variation in size of nanoparticle with

flowrate. The variation in average weight of resuspended particle with flowrate is shown in Table 4.2.

Table 4.2 Variation in average weight of nanoparticle removed with flow rate

Flow rate (l/min)	Avg. weight of removed particle (100 fg)
1.0	12.5
1.3	22.5
1.5	43.0
1.8	18.5
2.1	10.0
2.4	12.5
2.9	20.5

The effect of flowrate on the average weight of the nanoparticle can be divided into three regions, which are depicted in Fig. 4.5. The blue dashed curve shows a best-fit interpolation of the data (in yellow markers). We note that the data cannot be fit using a simple polynomial function of the flow rate. Region I in the figure refers to the flow rate regime where the average weight of the nanoparticles increases with the flow rate. This extends to a flow rate of 1.5 l/min. Region II refers to the regime where the average size decreases with increasing flow rate. This ranges from 1.5 to 2.1 l/min. Finally, in Region III that extends from 2.1 to 2.9 l/min, the average size of the removed nanoparticles increases again.

4.5 Discussion on results

We discuss the combined effect of flow rate on particle count and weight in this section. An overlay graph of the total particle count and the average particle weight with respect to flow rate is shown in Fig. 4.5.

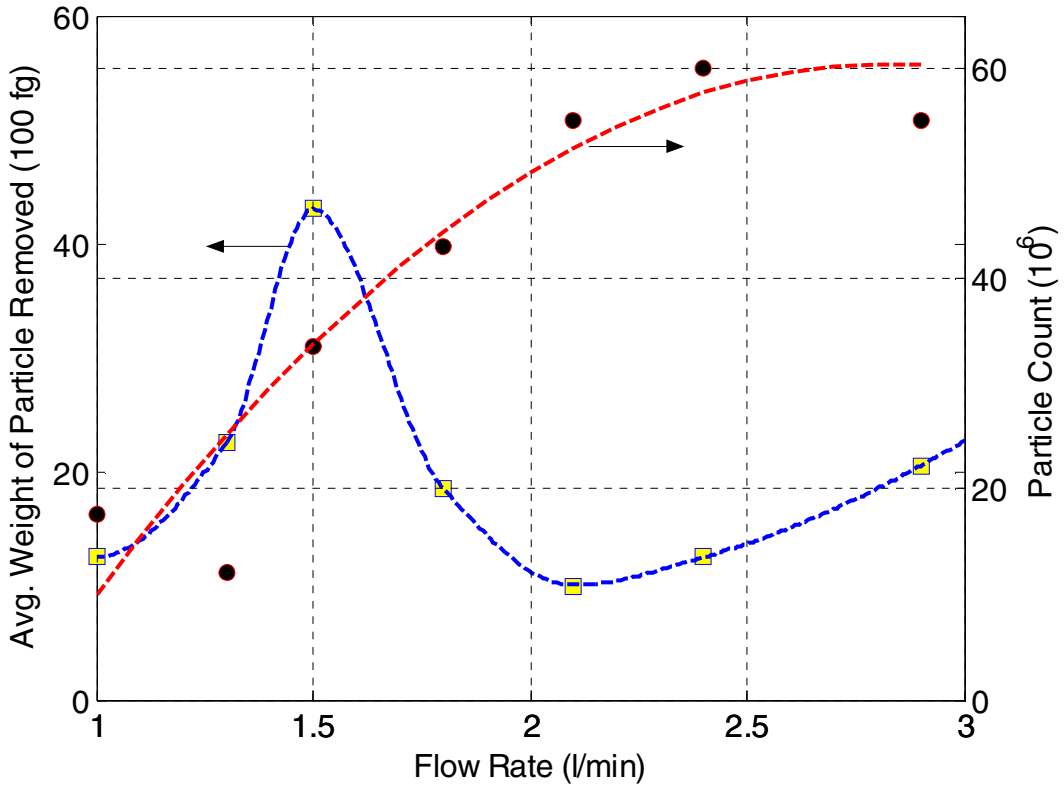

Fig. 4.5 Overlaid plot of variation of total particle count and weight of nanoparticles with increase in flow rate.

The resuspension of particles with respect to flow rate can be divided into three distinct regions. As discussed previously in Section 4.4.2, we make the assumption that the weight of a particle is proportional to its size. In other words, lighter particles are smaller and heavier are larger. The three regions of resuspension are as follows.

In Region I that extends from flow rates of 1.0 to 1.5 l/min, we observe that the particle count consistently increases while the average weight of the particle also increases. This means that, due to an increase in acceleration with increasing flow rate, an increasing number of larger particles are being removed. This region validates the force balance

model of resuspension according to which a particle gets removed when the acceleration due to the removal force is sufficient to instantaneously remove it.

In Region II that extends from flow rates of 1.5 to 2.1 l/min, we observe that the particle count continues to increase while the average weight of the nanoparticle decreases. This means that smaller particles are being removed in large numbers. The aerodynamic force is sufficient in this flow rate regime to remove smaller particles, which require higher flow rates. This region validates the energy balance model of resuspension according to which a particle accumulates energy from the removal force. When a particle gains enough energy to roll/slide (but insufficient to lift off the surface) it starts moving along the surface of the substrate. Finally, when it has accumulated sufficient energy to lift-off, it gets detached.

In Region III that extends from flow rates of 2.1 to 2.9 l/min, we observe that the average weight of the nanoparticle increases again with increasing flow rate. This means that primarily larger particles are being removed from the surface. This region validates the particle-wall collision model according to which particles agglomerate and collide with each other. This process of particle collisions with the surface leads to transfer of energy necessary for lift-off of the particle.

4.6 Limitations of the carbon experiments

The carbon particle experiments provide a good foundation for understanding resuspension from packed beds. However, in order to better understand the process, it is

necessary to identify and control the factors that introduce randomness and complexity (Wang 1991).

For example, the carbon nanoparticles have a broad range of size. This leads to a wide scatter in the adhesion force. Monodisperse spherical particles can address this issue. In particular, using commercially available silica nanospheres having a very narrow size range with a minimum standard deviation can overcome this limitation. The amount or number of nanoparticles on the surface of the carbon particles is also difficult to determine. However, this knowledge is necessary to ensure that there are a reasonable number of particles available for resuspension in the experiments.

The carbon particles were irregularly shaped making it very difficult to calculate the flow parameters. The use of spherical substrate microspheres addresses this problem. The carbon mixture was used in the experiment over a period of time. The residence time needs to be a minimum to prevent humidity from increasing the capillary condensation forces. Hence, it is necessary to monitor the temperature and humidity.

The roughness of the carbon particles varied from a few nanometers to 140 μm. This variability in roughness would unexpectedly influence the adhesion force thereby altering the resuspension. Hence, it is required to use microspheres that appear relatively "smooth" and the root mean square value of the roughness can be determined.

The carbon substrates break very easily and form a powder. This makes it difficult to study the substrate for roughness, size, surface potential and adhesion force. Further, it alters the count of nanoparticles that are available for resuspension. Hence, it is necessary

to use substrates that do not break easily and can be characterized using several surface measurement techniques.

In order to address these limitations, a series of controlled experiments using silica microspheres were conducted and are described in Chapter 5. Though the experiments discussed in the chapter suffer from control limitations owing to the use of carbon particles, the experience was helpful in designing the experiments on silica microspheres.

4.7 Summary

The carbon experiments validates the theoretical models, presents interesting results and limitations and essentially sets the stage for running a controlled set of silica experiments. The silica experiments study the effect of particle size on entrainment from surfaces. These are presented in Chapter 5.

CHAPTER 5 Effect of Size on Resuspension

This chapter discusses the effect of particle size and substrate size on resuspension. We use the experimental setup described in Chapter 3 to measure the fraction of detachment for different combinations of particle and substrate sizes. Detachment fraction is the ratio of the number of particles detached to the original number of particles that were present before the start of resuspension (Ibrahim, Dunn et al. 2003). Section 5.1 qualitatively discusses the expected influence of particle size based on existing theory. We present characterization results for the substrate in Section 5.2 in terms of the surface roughness of the substrate beads and their adhesive forces. Sections 5.3 and 5.4 present measured detachment fractions for different combinations of particle and substrate sizes. Section 5.3 describes a set of experiments in which the substrate size is kept constant while the particle size is varied. In the second set of experiments, reported in Section 5.4, we study the effect of substrate size on resuspension by keeping the particle size constant and varying the substrate size. Finally, we summarize and discuss the experimental results in Section 5.5.

5.1 The Predicted Effect of Size

The resuspension of a particle from the surface of the substrate depends on the complex interaction between the nanoparticles and the micrometer-size substrate. The

detachment flux is an important measure of the micro-nano particle interaction that can be studied in a controlled set of conditions. Since in all the experiments reported below, the interstitial velocity is set constant at 101 m/s, it follows that the aerodynamic force applied to a particle is the same. Section 3.3.4 has the details of the interstitial velocity calculation. However, from Section 2.3, it can be inferred that with decreasing particle size, the removal force increases. To determine the detachment flux the raw count of released particles is corrected for different values of surface density of nanoparticles using the method outlined in Chapter 3.

Hence, the detachment flux is expected to increase with the size of the nanoparticle. Therefore, for the three sizes of the nanoparticles used in this work, the detachment rate decreases in the order: 970 nm > 570 nm > 330 nm. Further, the size of the substrate has no effect on detachment flux, because it has been approximated as a flat surface.

5.2 Substrate Characterization

As discussed in Chapter 2, parameters such as the volumetric flow rate, the Reynolds number, the pressure drop across the tube, the size of the substrate particles, the resistance coefficient and the porosity of the bed determine the interstitial velocity of air through the mixture of substrate and nanoparticles. Of the methods mentioned in the literature review, we choose a combination of Darcy and Idelchik methods to calculate the flow parameters. With reference to Section 2.4, we understand that the Idelchik method is used because it is valid for both laminar and turbulent regime. The method to calculate the porosity, pressure difference, Re number and interstitial velocity is outlined in Section

2.4.1 and 2.4.2. As discussed in Chapter 2, the porosity of a bed of spherical bodies is independent of the diameter of the grain while the relative position of the grains varies from 60 to 90^0. Using these values in Eq 2.13, we estimate the porosity, ε ' to be in the range 0.25 - 0.47. Table 5.1 lists the porosity values for different grain disposition angle, θ .

Table 5.1 Porosity as a function of the grain disposition angle

θ	60^0	64^0	69^0	74^0	81^0	90^0
ε '	0.26	0.32	0.38	0.42	0.46	0.47

Using the Idelchik method, the permeability of the bed can be determined. The permeability of the bed is determined rather than the conductivity, because permeability is a property of the bed while the conductivity is a property of the fluid. After determining the permeability, the Idelchik method is used as outlined in Section 2.4 to determine the flow parameters. In the set of experiments described below, the volumetric flow rate is varied with respect to the size of the microspheres to maintain the interstitial velocity at 101 m/s (refer Section 3.3.4).

Table 5.2 Flow parameters interstitial velocity is 101 m/s

Median substrate size (μm)	Flow rate (l/min)	Re number
648	11.7	5211-5440
360	8.2	2895-3022
272	4.9	2187-2283

Further, as discussed in Section 3.3, it is clear that the surface of the substrate sphere can be approximated as a flat surface. The surface roughness of a substrate determines the area of contact with the nanoparticle, and, in turn, affects the van der Waals surface adhesive force. Table 5.3 lists the root mean square height (R_q) of the roughness of the surface (refer Section 3.3.2).

Table 5.3 Roughness of the substrate beads

Size of substrate (μm)	Surface roughness (nm)
590-840	123
350-500	100
250-350	155

The adhesive force is measured using an atomic force microscope (AFM). The method to calculate the AFM force measurements is described with reference to Fig. 5.1.

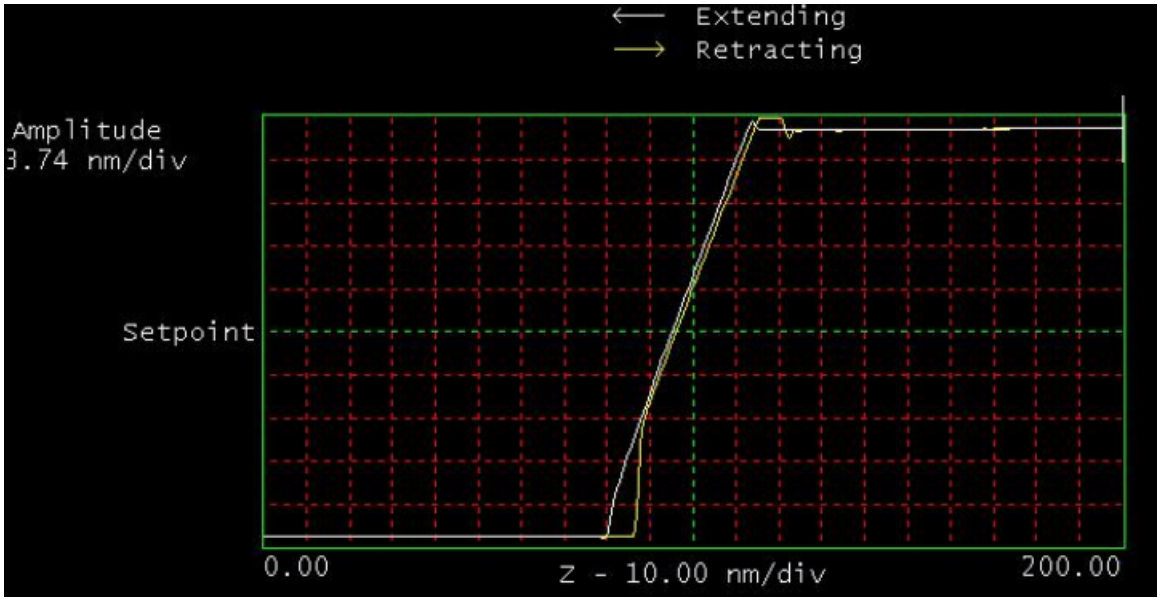

Fig. 5.1 AFM force calibration plot measurement

The deflection of the tip of the AFM is proportional to the attractive force acting between the tip and the surface. This relation is given by Hooke's law

$$F = k_2 x \tag{5.1}$$

where F is the deflection force, k_2 is the spring constant and x is the extent of deflection.

The sensitivity of the curve should be calibrated to measure the correct deflection. The inverse of the slope of the force curve is the sensitivity. The slope is determined by drawing a line parallel to the force curve. The number of divisions that are present between the tip touching the surface and the point where it feels no attraction is obtained from the plot. Then we determine the deflection by multiplying the sensitivity with the number of deflection divisions and the z-axis (nm/div). The spring constant of the AFM tip is a range of values. The product of the spring constant with the deflection gives the range of attractive forces (Sharma, Chamoun et al. 1992; Das, Schechter et al. 1994). However, it is difficult to determine the adhesive force precisely since it is a function of the geometry and material of the AFM tip and cantilever (Freitas and Sharma 2001). However, a qualitative understanding can be obtained by repeating the measurements over several areas of the substrate. Table 5.4 tabulates the range of surface adhesive force exerted on the tip by substrates of different sizes.

Table 5.4 Measured surface adhesive force for different sizes of the substrate beads

Size of substrate (μm)	Adhesive force$_{min}$(nN)	Adhesive force$_{max}$(nN)
590-840	330	1138
350-500	255	1023
250-350	242	970

5.3 Measured Effect of Particle Size

In this section, we present experimental data for the fraction of detachment when the substrate size is kept same while the particle size is varied. The first three subsections present results for the three different bead sizes which are characterized in Section 5.2 above. Subsection 5.3.4 combines the experimental results from the three sets and compares them with theoretical predictions based on surface property measurements.

5.3.1 Results for Large Substrate Particles (590-840 μm silica beads)

For a bed composed of 590-840 μm sized silica beads (the substrate), the variation in fraction of detachment of nanoparticles due to variation in nanoparticle size is tabulated in Table 5.5 and shown in Fig. 5.2.

Table 5.5 Fraction of detachment for 590-840 μm spheres

Particle (nm)	Raw count	Detachment flux/m^2	Number of particles/m^2	Fraction of detachment
330	9.6×10^{3}	0.55×10^{7}	3.8×10^{13}	1.5×10^{-7}
570	5.2×10^{3}	3.05×10^{6}	7.4×10^{12}	4.1×10^{-7}
970	7.6×10^{3}	4.50×10^{6}	1.5×10^{12}	3.0×10^{-6}

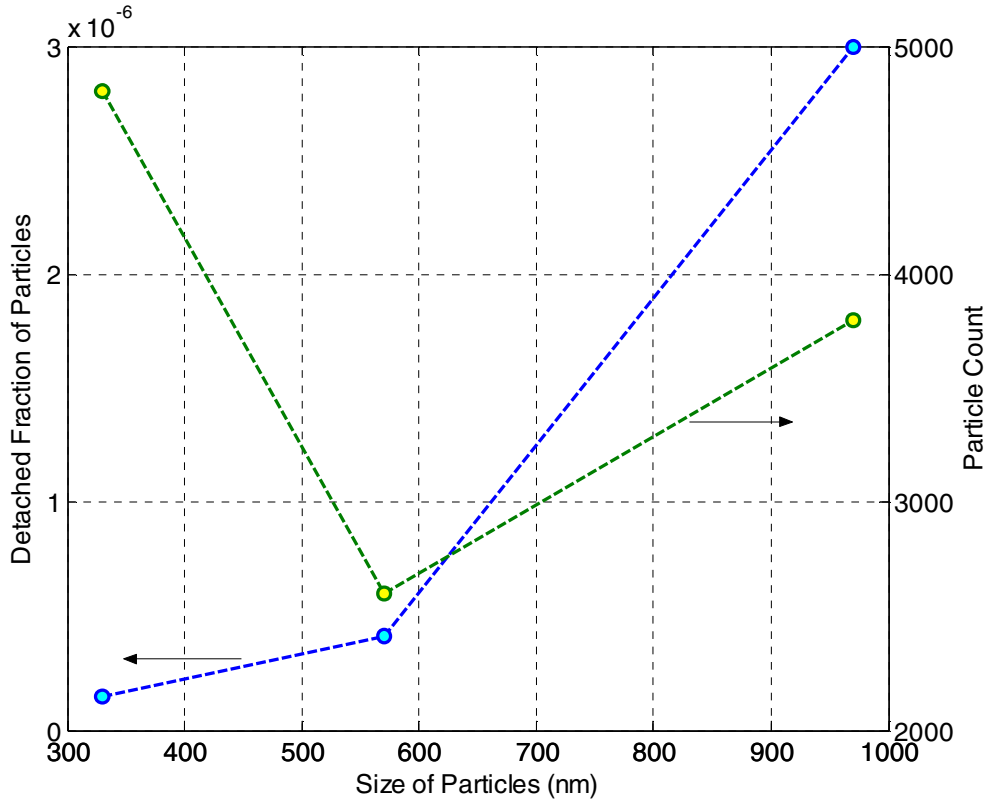

Fig 5.2 Variation in fraction of detachment of nanoparticles on 590-840 μm substrate

As the particle size increases the fraction of detachment also increases. The rms value of roughness is 123 nm (Table 5.3) and the mean value of adhesive force is 330-1138 nN (Table 5.4).

5.3.2 Results for Medium Substrate Particles (350-500 μm silica beads)

For a bed composed of 350-500 μm sized silica beads (the substrate), the variation in fraction of detachment of nanoparticles due to variation in nanoparticle size is tabulated in Table 5.6 and shown in Fig. 5.3.

Table 5.6 Fraction of detachment for 350-500 μm spheres

Particle (nm)	Raw count	Detachment flux/m^2	Number of particles/m^2	Fraction of detachment
330	2.4×10^{5}	0.70×10^{8}	2.1×10^{13}	3.35×10^{-6}
570	8.9×10^{4}	2.60×10^{7}	4.1×10^{12}	0.65×10^{-5}
970	6.1×10^{4}	1.75×10^{7}	8.3×10^{11}	2.15×10^{-5}

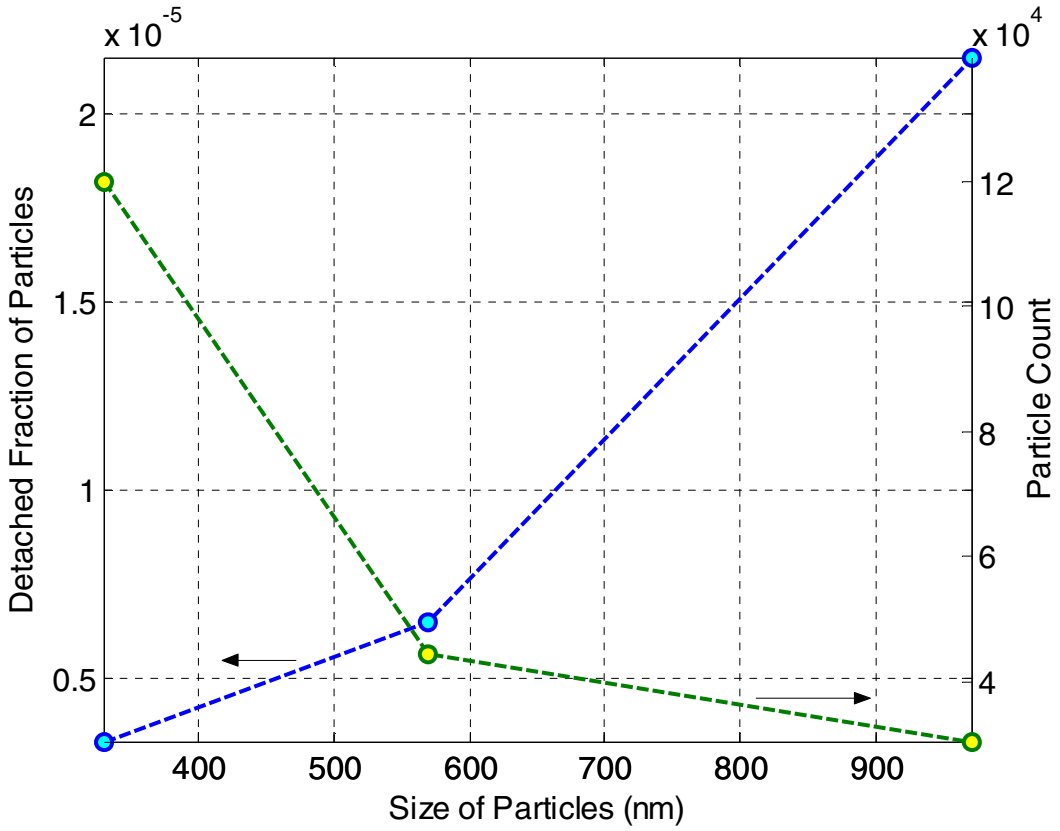

Fig 5.3 Variation in fraction of detachment of nanoparticles on 350-500 μm susbtrate

As the particle size increases the fraction of detachment also increases. The rms value of roughness is 100 nm (Table 5.3) and the mean value of adhesive force is 255-1023 nN (Table 5.4).

5.3.3 Results for Small Substrate Particles (250-350 μm silica beads)

For a bed composed of 250-350 μm sized silica beads (the substrate), the variation in fraction of detachment of nanoparticles due to variation in nanoparticle size is tabulated in Table 5.7 and shown in Fig. 5.4.

Table 5.7 Fraction of detachment for 250-350 μm spheres

Particle (nm)	Raw count	Detachment flux/m^2	Number of particles/m^2	Fraction of detachment
330	1.5×10^{5}	3.15×10^{7}	1.6×10^{13}	1.95×10^{-6}
570	1.2×10^{5}	2.50×10^{7}	3.1×10^{12}	0.80×10^{-5}
970	1.0×10^{5}	2.20×10^{7}	6.3×10^{11}	3.45×10^{-5}

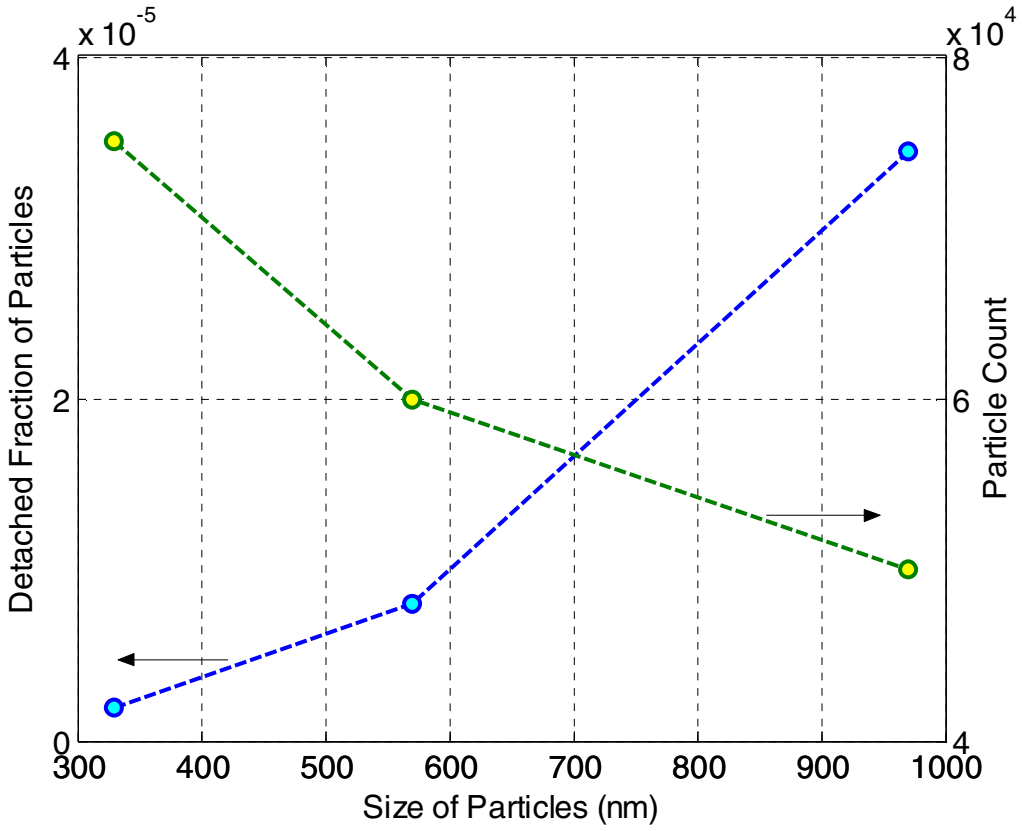

Fig 5.4 Variation in fraction of detachment of nanoparticles on 250-350 μm susbtrate

As the particle size increases the fraction of detachment also increases. The rms value of roughness is 155 nm (Table 5.3) and the mean value of adhesive force is 242-970 nN (Table 5.4).

5.3.4 Analysis – Influence of Size of Nanoparticles

Tables 5.5, 5.6 and 5.7, show that the fraction of detachment increases as the size of the nanoparticle increases, irrespective of the size of the substrate. This is summarized in Fig. 5.5, which is the overlay graph of all 9 combinations of mixtures.

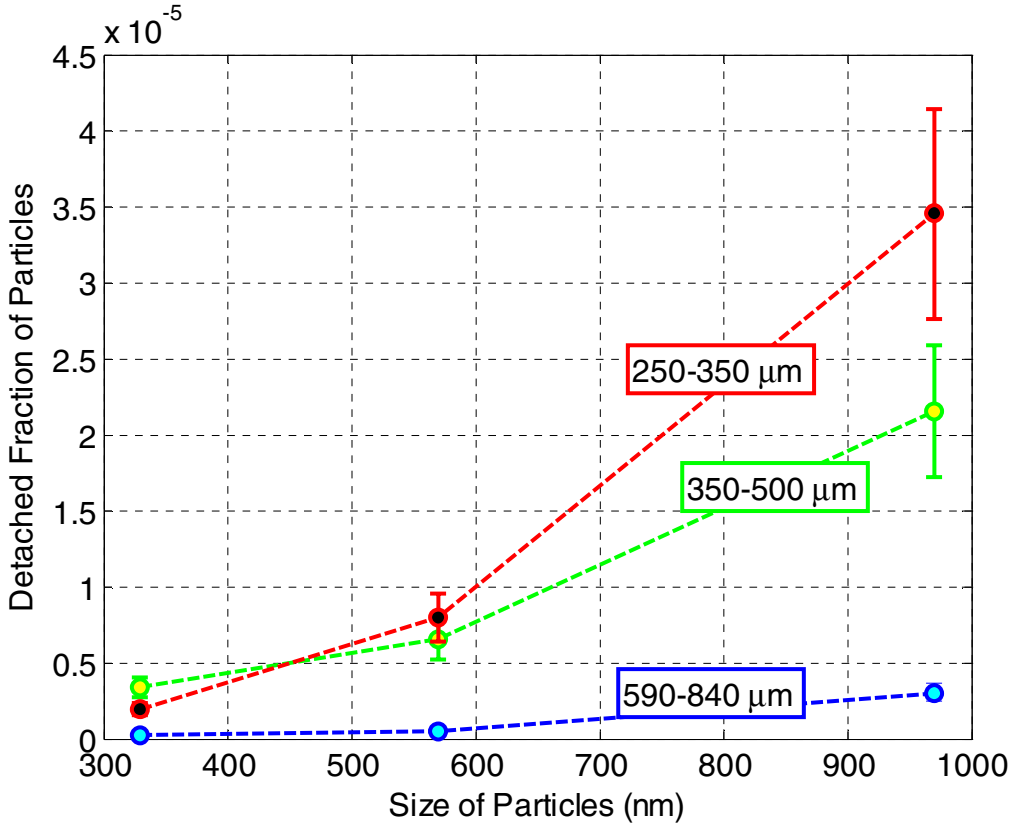

Fig. 5.5 Variation in detachment fraction of nanoparticles as a function of the size of the nanoparticles.

The results are in accordance with the theory of attachment and resuspension of nanoparticles on surfaces. The van der Waals attractive force is most dominant in the case of particles below 50μm. The van der Waals moment increases quadratically with the particle diameter as given by Eq. 2.11. The drag moment increases as the cube of the diameter. Hence, the ratio of the removal force to the attractive force increases with particle size. However, we note that the observed increase in detachment fraction is non-linear with respect to particle size and not linear as the ratio of the two moments might suggest.

5.4 Measured Effect of Substrate Size

In this section, the effect of substrate size on the resuspension process is discussed. Theory conveys that the surface of the microsphere is like a flat surface for the nanometer sized beads. Hence, the size of the substrate should not have any effect on the attachment and detachment characteristics of the nanoparticles. However, a comparison of nanoparticle resuspension with change in substrate size conveys that the substrate size and surface roughness are important factors. This is demonstrated in Fig. 5.6.

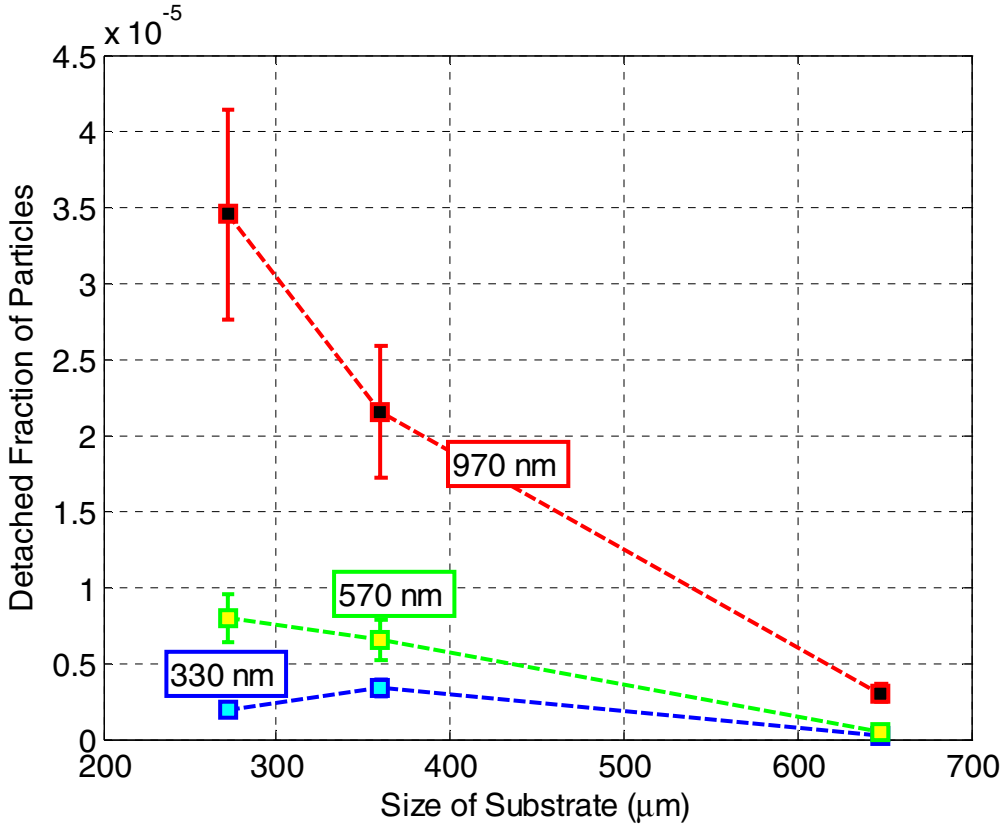

Fig. 5.6 Variation in detachment fraction of nanoparticles due to size of substrate

In the case of 570 and 970 nm particles, the resuspension decreases with increase in size of the substrate beads. This can be explained from the AFM surface force measurements (refer Table 5.4). Hence, as the size of the substrate increases, for larger size nanoparticles (570 and 970 nm), the adhesive force increases thereby reducing detachment rate.

For the 330 nm particles on substrates of different sizes, the variation in resuspension is due to difference in roughness profile of the microspheres. From Table 5.3, it is understood that the 250-350 µm beads have a roughness of 155 nm, followed by the

590-840 μm beads with 123 nm and the smoothest are the 350-500 μm beads with a mean roughness of 100 nm. The resuspension is lesser for 330 nm particles on 250-350 μm susbtrate beads because the surface roughness is close to the order of magnitude of the nanoparticles. Hence, the nanoparticles reside in the valleys on the surface thereby decreasing resuspension. For larger sized nanoparticles (570 and 970 nm), the order of magnitude of the nanoparticles is less than that of the surface roughness. With increase in roughness of the surface, the area of contact with the nanoparticles decreases, hence the adhesive force also falls, leading to an increase in resuspension rate.

5.5 Closure

This chapter presented data from resuspension experiments on silica microspheres and nanoparticles. We find the detachment fraction to increase with increasing particle size for all the three substrate sizes investigated. We attribute this to the increase in drag moment with particle size. However, we find that the detachment fraction grows non-linearly with particle diameter whereas a ratio of the drag moment to the van der Waal's moment suggests a linear increase. Finally, we find the substrate size to also influence the detachment fraction. The detachment fraction decreases with an increase in the substrate size. We attribute this to the surface roughness being comparable to the particle size in our measurements.

CHAPTER 6 Conclusions and Future Work

6.1 Conclusion

The carbon set of experiments validated the force balance and energy balance models of nanoparticle entrainment from surfaces. It was observed that the particle size and shape affected the flow parameters, thereby introducing variability in the resuspension rates. The energy balance model, with the rock'n roll modification, correlated better with the experimental results. The count of removed particles increased significantly with the flow rate ($\alpha = 0.95$, p-value < 0.0076). The empirical relation describing the effect of flow rate on the particle size is $n(10^6) = -15 f_1^2 + 85 f_1 - 60$, where n is the particle count and f_1 is the flow rate in *l*/min. The carbon study identified the limitations and set the stage for controlled silica trials.

The silica experiments, had nanometer sized spheres on the surface of micron-sized silica beads. The sizes of the nano and micro-sized spheres were varied and its effect on the detachment fraction was recorded. The detachment fraction increased with increasing particle size for all the three sizes of substrate. This is a result of the increase in drag moment with increasing particle size. Further, we observed that the detachment fraction grows non-linearly with particle diameter whereas a ratio of the drag moment to the van der Waal's moment suggests a linear increase. Finally, we find that the substrate size also influences the detachment fraction. The detachment fraction decreases with an increase in

the substrate size. This is due to the surface roughness being of the same order of magnitude of the particle size. When the substrate size is large, the asperities on its surface do not affect the resuspension. However, as the substrate size decreases and the nanoparticle dimension gets closer to the size of the asperity, detachment fraction decreases.

6.2 Areas for future study

The surface roughness measurements would provide more information if studied for nanoparticle sizes lesser than 330nm. It was difficult to study that because as the size of the nanoparticle decreased, its agglomeration increased and the range of size was not narrow. Current theoretical models do not account for the influence of surface roughness on the resuspension process.

It will be useful to study the behavior of the particle after it is entrained. Studying the dynamics of the particle will provide information on what mechanism was responsible for entrainment, mode of motion after detachment (sliding or rolling), whether the particle got attached again to the surface and what caused it.

Further, including the study of factors like residence time and humidity of nanoparticles would provide useful information about the entrainment process.

Literature Cited

Adhiwidjaja, I., S. Matsusaka, et al. (2000). "Simultaneous Phenomenon of Particle Deposition and Reentrainment: Effects of Surface Roughness on Deposition Layer of Striped Pattern." Aerosol Science & Technology **33**(4): 323-333.

Akiyama, T. and Y. Tanijiri (1989). "Criterion for re-entrainment of particles." Powder Technology **57**(1): 21-26.

Bhattacharya, S. and K. L. Mittal (1978). "Mechanics of removing glass particulates from a solid surface." Surface Technology **7**(5): 413-425.

Bowling, A. (1988). "Particles on Surfaces 1 Detection, Adhesion and Removal."

Cheng, W., P. F. Dunn, et al. (2002). "Surface roughness effects on microparticle adhesion." Journal of Adhesion **78**.

Cheng, W., P. F. Dunn, et al. (2003). "Contact between a smooth microsphere and an anisotropic rough surface." The Journal of Adhesion **79**.

Cleaver, J. W. and B. Yates (1973). "Mechanism of detachment of colloidal particles from a flat substrate in a turbulent flow." Journal of Colloid and Interface Science **44**(3): 464-474.

Corn, M. J. (1961). "The adhesion of solid particles to solid surfaces II." Journal of air pollution control association **11**: 566-575.

Das, S. K., R. S. Schechter, et al. (1994). "The Role of Surface Roughness and Contact Deformation on the Hydrodynamic Detachment of Particles from Surfaces." Journal of Colloid and Interface Science **164**(1): 63-77.

Denis J. Phares;Gregory T.. Smedley, R. C. F. (2000). "Effect of particle size and material properties on aerodynamic resuspension from surfaces." Journal of Aersol Science **31**(11): 1335-1353.

Freitas, A. M. and M. M. Sharma (2001). "Detachment of Particles from Surfaces: An AFM Study." Journal of Colloid and Interface Science **233**(1): 73-82.

Friedlander, S. K. (2000). Smoke, Dust, and Haze. New York, Oxford University Press.

Friess, H. and G. Yadigaroglu (2002). "Modelling of the resuspension of particle clusters from multilayer aerosol deposits with variable porosity." Journal of Aerosol Science **33**(6): 883-906.

Gotoh, K., K. Karube, et al. (1996). "High-efficiency removal of fine particles deposited on a solid surface." Advanced Powder Technology **7**(3).

Hoenig, S. A. (1986). Particles on surfaces 1 : detection, adhesion, and removal. San Francisco, Plenum Press.

Ibrahim, A. H., P. F. Dunn, et al. (2003). "Microparticle detachment from surfaces exposed to turbulent air flow: controlled experiments and modeling." Aerosol Science **34**.

Ibrahim, A. H., P. F. Dunn, et al. (2004). "Microparticle detachment from surfaces exposed to turbulent air flow: Effects of flow and particle deposition characteristics." Journal of Aerosol Science **35**(7): 805-821.

Idelchik, I. E. and E. Fried (1986). Handbook of Hydraulic Resistance. New York, Hemisphere Publishing Corporation.

Israelachvili, J. N. (1985). " Intermolecular and surface forces : with applications to colloidal and biological systems."

Israelachvili, J. N. (1992). Intermolecular and surface forces. San Diego, Academic Press.

Johnson, K. L., K. Kendall, et al. (1971). "Surfac eenergy and contact of Elastic solids." Proceedings of the Royal Society of London, Series A, Mathematical and Physical Sciences **324**.

Jurcik, B. and H.-C. Wang (1991). "The modeling of particle resuspension in Turbulent flow." Journal of Aerosol Science **22**.

Kaviany, M. (1999). Principles of heat transfer in porous media, Springer.

Lazaridis, M. and Y. Drossinos (1995). "Resuspension of small particles by turbulent flow." Journal of Aerosol Science **26**.

Lazaridis, M., Y. Drossinos, et al. (1998). "Turbulent Resuspension of Small Nondeformable Particles." Journal of Colloid and Interface Science **204**(1): 24-32.

Matsusaka, S. and H. Masuda (1996). "Particle reentrainment from a fine powder layer in a turbulent air flow." Aerosol Science & Technology **24**: 69-84.

Mollinger, A. M., F. T. M. Nieuwstadt, et al. (1992). "Entrainment of particles in a turbulent boundary layer, evaluation of the forces on a single particle." Journal of Aerosol Science **23**(1).

Nicholson, K. W. (1988). "A review of particle resuspension." Atmospheric Environment **22**(12).

Phares, D. J., G. T. Smedley, et al. (2000). "Effect of Particle size and material properties on aerodunamic resuspension from surfaces." Journal of Aerosol Science **31**(11): 1335-1353.

Ranade, M. B. (1987). "Adhesion and Removal of Fine particles on surfaces." Aerosol Science and Technology **7**.

Reeks, M. W. and D. Hall (2001). "Kinetic models for particle resuspension in turbulent flows: theory and measurement." Journal of Aerosol Science **32**(1): 1-31.

Reeks, M. W. R. J. R. H. D. (1988). "The resuspension of small particles by a turbulent flow." Journal of Physics D **21**: 574-589.

Reeks, M. W. R. P. (1988). "The adhesion of small particles to a surface." Proceedings of the second conference of the aerosol society.

Sharma, M. M., H. Chamoun, et al. (1992). "Factors controlling the hydrodynamic detachment of particles from surfaces." Journal of Colloid and Interface Science **149**(1): 121-134.

Stein, C. M. F. (1965). "Re-entrainement of particles from a plane surface." American Industrial Hygiene Association **26**: 325-336.

Theerachaisupakij, W., S. Matsusaka, et al. (2003). "Reentrainment of deposited particles by drag and aerosol collision." Journal of Aerosol Science **34**(3): 261-274.

Wang, H.-C. (1990). "Effects of inceptive motion on particle detachment from surfaces." Aerosol Science & Technology **13**: 386-393.

Wang, H.-C. (1991). Particles on surfaces 3 : detection, adhesion, and removal. San Diego, Plenu Press.

Wen, H. Y. and G. Kasper (1989). "On the kinetics of particle reentrainment from surfaces." Journal of Aerosol Science **20**(4): 483-498.

Wen, H. Y., G. Kasper, et al. (1989). "Short and long term particle release from surfaces under the influence of gas flow." Journal of Aerosol Science **20**(8): 923-926.

White, F. M. (2003). Fluid Mechanics, Mc Graw Hill.

Ziskind, G., M. Fichman, et al. (1995). "Resuspension of particulates from surfaces to turbulent flows--Review and analysis." Journal of Aerosol Science **26**(4): 613-644.

Ziskind, G., M. Fichman, et al. (1997). "Adhesion moment model for estimating particle detachment from a surface." Journal of Aerosol Science **28**(4): 623-634.

APPENDIX A Uncertainty Analysis

Let the detached fraction be φ and let the uncertainty be denoted by u.

Now,

$$\varphi = \frac{n_C}{P},$$

where n_c is the raw count of detached particles and P is the number of particles added to the substrate. Also,

$$P = \frac{W_p}{\rho_p \frac{4}{3}\pi r_p^{\,3}},$$

where W_p is the weight of nanoparticles added to the mixture, ρ_p is the density and r_p is the average radius of the particle. The uncertainty in the measured detachment fraction is thus,

$$u_\varphi = \sqrt{u_{n_c}^2 + u_{W_p}^2 + 3u_{r_P}^2} \quad .$$

The instrument manual for the particle counter, TSI 3022A states that u_{n_c} is 0.20. The manual for the weighing balance, and GR-202 states that u_{W_p} is 0.1 mg in 500 mg or $2\text{x}10^{-3}$. Finally, u_{r_P} is 1 µm in 970 µm or $1\text{x}10^{-3}$. Thus, we see that the dominant contribution to the experimental uncertainty is from the particle counter. The net uncertainty is approximately ±20%.

VITA

Education

M.S. (Engineering) Virginia Commonwealth University, Richmond, VA
Dec 2006 **GPA: 4.0**
B.S. (Electronics) R.V. College of Engineering, Bangalore, India
July 2002 **GPA: 3.8**

Work Experience

Co-op Intern Research, Development and Engineering Division, Philip Morris
Jan '06-Oct '06

- Measured and analyzed aerosol properties, sub-micron surface properties and interactions of particles

Research Asst. Energy Conversion Systems Lab, Virginia Commonwealth University
Nov '04-Dec '06

- Conducted experiments on nanoparticle resuspension in turbulent flows, demonstrated the working of different models, and showed the different mechanisms that effect particle resuspension based on size of particle

Teaching Asst. Mechanical Engineering, Virginia Commonwealth University
Fall 2005

- Assisted 75 seniors in a course on Mechanical Electronics

Software Engineer DayBegins Engineering Innovations, Bangalore, India
Dec '02-July '04

- Worked on the development of an Internet and Network security product.

Research Asst. Indian Space Research Organization, Bangalore, India Dec '01-July '02

- Studied various digital modulation methods and developed a working model of the OQPSK and BPSK schemes

Awards and Achievements

- Ranked in top 2% of undergraduate class (1996-2000)
- Nationwide science scholarship and medal from Central Institute of General Knowledge Learning, New Delhi (1994-96)
- Awarded the Asha Melmane Shield for the "Best Science Student" in high school (1994)